Summer 7-2016

The Influence of Relative Particle Size and Material Interactions on the Flow-Induced Detachment of Particles from a Microchannel

Morgan Brittany Mayfield
Rose-Hulman Institute of Technology, mayfiemb@rose-hulman.edu

The Influence of Relative Particle Size and Material Interactions on the Flow-Induced Detachment of Particles from a Microchannel

A Thesis

Submitted to the Faculty

of

Rose-Hulman Institute of Technology

By

Morgan Brittany Mayfield

In Partial Fulfillment of the Requirements for the Degree

of

Master of Science in Chemical Engineering

July 2016

ROSE-HULMAN INSTITUTE OF TECHNOLOGY

Final Examination Report

Morgan B. Mayfield — Name

Chemical Engineering — Graduate Major

Thesis Title: The Influence of Relative Particle Size and Material Interactions on Flow-Induced Detachment of Particles from a Microchannel

DATE OF EXAM: July 19, 2016

EXAMINATION COMMITTEE:

	Thesis Advisory Committee	Department
Thesis Advisor:	Kimberly Henthorn	CHE
	Adam Nolte	CHE
	Daniel Morris	CHEM

PASSED X **FAILED** _____

ABSTRACT

Mayfield, Morgan Brittany

M.S.Ch.E.

Rose-Hulman Institute of Technology

July 2016

The Influence of Relative Particle Size and Material Interactions on the Flow-Induced Detachment of Particles from a Microchannel

Thesis Advisor: Dr. Kimberly Henthorn

Particulate transport in microfluidic channels is difficult due to confined geometries and low flow rates, which promote solids settling. To re-entrain these solids, the detachment behavior of closely-fitting particles from microchannel walls must be understood. Experiments were completed to examine the effects of particle size and material interactions on particle detachment velocity. Studies were conducted for various sizes of glass and poly(methyl methacrylate), PMMA, spheres in glass and poly(dimethyl siloxane), PDMS, microfluidic channels. In addition, an inexpensive method to produce monodisperse PMMA microparticles was developed. To analyze the effect of material interactions, the work of adhesion between the particle and the channel wall was calculated. The fluid velocity required to detach a particle was found to be relatively constant until the particle-to-channel diameter ratio approached approximately 50%, after which detachment velocity decreased with increasing particle size. Particles in a glass microchannel experienced significantly more adhesion than those in PDMS channels.

Keywords: Chemical engineering, microfluidics, microparticle detachment, work of adhesion

ACKNOWLEDGEMENTS

I would first like to thank my thesis advisor, Dr. Kimberly Henthorn. She has been an immense help through every step of this process and I have loved working with her. Dr. Kim has been a source of invaluable support and guidance while letting me make this project my own. I truly could not have asked for a better mentor. Aside from my advisor, I would like to thank the other members of my thesis committee, Dr. Adam Nolte and Dr. Daniel Morris, for always being willing to answer my questions and for pointing me in the right direction whenever I lost sight of my next step. I would also like to thank our department's laboratory technician, Frank Cunning. Not only did he provide all of the supplies and every piece of equipment needed to complete this project, but his sunny disposition and support helped me stay positive through the most frustrating parts of this process. I would also like to thank Dr. David Henthorn and Dr. Luanne Tilstra for their assistance and allowing me to use the resources at their disposal.

Finally, I must express my gratitude to my family and friends for supporting me through this entire process. Without their patience and advice, this thesis would not have been possible. As we go our separate ways, I am truly going to miss every member of my Rose-Hulman family and I wish you all the best.

Thank you,

Morgan Mayfield

TABLE OF CONTENTS

Contents

LIST OF FIGURES

Figure Page

LIST OF TABLES

Table Page

LIST OF ABBREVIATIONS

CFD	Computational fluid dynamics
DMPA	2,2-dimethoxy-2-phenylacetophenone
EGDMA	Ethylene glycol dimethacrylate
GMA	Glycidyl methacrylate
IBA	Isobornyl acrylate
JKR	Johnson, Kendall, and Roberts
MC	Methyl cellulose
MEMS	Micro electrical mechanical systems
MMA	Methyl methacrylate
MTMP	2-methyl-4′-(methylthio)-2-morpholinopropiophenone
PCMR	Polymerase chain reactions
PDMS	Poly(dimethyl siloxane)
PIBA	Poly(isobornyl acylate)
PMMA	Poly(methyl methacrylate)
PVA	Poly(vinyl alcohol)
SiO_2	Silica, or silicon dioxide
UV	Ultraviolet

LIST OF SYMBOLS

English Symbols

A_H	Hamaker constant
a_{eq}	Particle's contact diameter with the channel wall
Ca	Capillary number
D_i	Diameter of the inner channel in the droplet-forming microfluidic device
D_o	Diameter of the outer channel in the droplet-forming microfluidic device
d_c	Diameter of the channel
d_p	Diameter of the particle
$d_{p,eff}$	Effective diameter of the particle
$d_{p,eff,sphere}$	Effective diameter of a sphere in contact with another sphere
$d_{p,eff,plane}$	Effective diameter of a sphere in contact with a flat plane
E_1	Young's modulus of the particle
E_2	Young's modulus of the channel
F_A	Force due to adhesion
$F_{A_{JKR}}$	Force due to adhesion calculated using the JKR theory
$F_{A_{van\ der\ Waals}}$	Force due to van der Waals adhesion
F_B	Force due to buoyancy
F_D	Force due to drag
F_F	Force due to friction
F_G	Force due to gravity

F_L	Force due to lift
F_{shear}	Shear viscous forces acting on a growing droplet
F_γ	Force due to the interfacial tension between two immiscible liquids
g	Acceleration due to gravity
K	Composite Young's modulus
k_1	Elastic coefficient of the particle
k_2	Elastic coefficient of the channel
M_{EffD}	Moment due to the effective drag of the fluid
M_F	Moment due to friction
n	Number of particles in a sample
Q	Volumetric flowrate required to detachment the particle
Q_1	Volumetric flowrate of the inner fluid in the droplet-forming microfluidic device
Q_2	Volumetric flowrate of the outer fluid in the droplet-forming microfluidic device
RM	Rolling moment
s	Spacing between a sphere and a flat surface
u	Velocity of the fluid
u_s	Settling velocity of a particle
u_1	Velocity of the inner fluid in the droplet-forming microfluidic device
u_2	Velocity of the outer fluid in the droplet-forming microfluidic device
V_p	Volume of the particle
W_A	Work of adhesion

Greek Symbols

α	Deformation at the interface between the particle and the channel
γ_1	Surface energy of the particle
γ_2	Surface energy of the channel
$\gamma_{1,2}$	Interfacial tension between two materials
μ	Dynamic viscosity of the fluid
μ_2	Dynamic viscosity of the outer fluid in the droplet-forming microfluidic device
ν_1	Poisson's ratio of the particle
ν_2	Poisson's ratio of the channel
ρ_f	Density of the fluid
ρ_{glass}	Density of glass
ρ_{PMMA}	Density of poly(methyl methacrylate)
ρ_p	Density of the particle

1. INTRODUCTION AND BACKGROUND

MEMS, or micro electrical mechanical systems, are becoming more prevalent and are currently used in many everyday applications, including air bag sensors, inkjet printers, and micro scale gyroscopes to name a few [1]. One subset of MEMS is microfluidics, which is revolutionizing chemical and biological analysis. Chemical systems scale down to the micro scale very favorably, with advantages such as smaller sample sizes, faster reaction kinetics, and more precise detection resolution. Microfluidic devices are used extensively in the medical field, particularly for genetic sequencing, medical diagnostics, and drug discovery [2]. One of the most popular "lab-on-a-chip" applications is DNA amplification through polymerase chain reactions (PCR) [3]. However, while scaling these systems down is often beneficial, some problems arise when attempting to work with solids suspended in two-phase flow. Many of these solids that would ordinarily be suspended in a bulk fluid are of comparable size to most microchannels, resulting in frequent contact between the particle and the channel. If the fluid is not flowing fast enough, these solids can settle to the bottom of the microchannel, causing blockages and impeding flow. To fix this problem, the fluid velocity must be adjusted to detach the particle from the wall and re-entrain it.

There are several situations where micro-scale solids need to flow through channels of a similar size. These can include everything from blood cells passing through capillaries to microreactors filled with packing materials. One specific application is the handling of livestock embryos. Gene manipulation and *in vitro* fertilization are becoming more common in the agricultural industry, but embryos are very fragile and difficult to handle individually. Instead,

microfluidic devices have been developed to transport and manipulate embryos, using fluid flow to roll embryos to different locations of the device for culturing and DNA analysis [4]. Due to the fragility of the system, a thorough understanding of the detachment behavior of large solids from microchannel surfaces is vital to avoid shocks and impacts that might harm the embryo.

While studies have been done in the past to characterize the detachment behavior of microparticles, few have been done in microfluidic channels. Most of the literature on the topic involves microparticle detachment in pneumatic conveying, where air is the propelling fluid and the geometry is unconstrained. The few studies that do concern microfluidics are primarily focused on the fundamental physics of the geometry and the forces acting on microparticles at the point of detachment. While the groundwork has been laid, there are still many unanswered questions, particularly about the adhesion forces and material interactions between the particle and the channel wall. This study will focus on characterizing the adhesion forces for various pairings of common materials used in microfluidics.

The materials examined in this study were chosen based on both relevance and ease of access. In general, microfluidic devices are made from either glass or poly(dimethyl siloxane), commonly known as PDMS. Each material has its own advantages and disadvantages for different applications, but both are easy to manipulate on a micro-scale and are inexpensive, making them the most popular options and the most relevant choices for this study. The decision of which microparticle materials to study was significantly more difficult. The first material chosen was glass, because not only are glass microparticles commercially available for purchase, glass is a common packing material and microspheres are frequently used as fillers and spacers.

For the second material, a flexible polymer was originally desired to model the flexible nature of most biological solids. The initial proposal for this project was to synthesize fluid filled polymer capsules that could flex and make contact with a larger portion of the microchannel. While this was attempted, there were setbacks throughout the course of the study and it was eventually decided to abandon the concept in favor of producing solid polymer spheres. These solid particles were made from poly(methyl methacrylate), known as PMMA or Plexiglas. PMMA was chosen because it is a conventional polymer widely used in everyday life. However, while PMMA microspheres are commercially available for purchase, they are prohibitively expensive and it is far more economical to synthesize the particles in-house. This lead to the second goal of this study: to find a simple and inexpensive method to produce monodisperse spherical polymer microparticles.

Polymer microparticles have been studied extensively, particularly for drug delivery applications. The use of polymer microparticles to deliver drugs can improve the circulation time of a drug, control the rate of drug release, protect the drug for acidic or enzymatic degradation, and allow for targeting to a specific area of the body, all of which are highly advantageous [5]. Most polymer microparticles are synthesized using an emulsion method, which is done by dissolving the polymer in an organic solvent and emulsifying it in an aqueous solution through mechanical stirring. Once the emulsification is complete, the organic solvent is removed through evaporation and the solid polymer microparticle is left. To create liquid filled particles, an emulsifying step first forms aqueous droplets in an organic phase. The organic phase is then added to another aqueous phase and emulsified, producing solid polymer particles containing the aqueous droplets emulsified in the first step. While this process is generally considered the

easiest option to produce large batches of microparticles, there are several drawbacks. The biggest problem for this application is the size variation in each emulsion batch. The size of the emulsified droplets depends primarily on the rate of stirring, but a variety of other factors also play a part, including the temperature and geometry of the stirring system [5]. Temperature gradients and imperfect mixing can cause significant polydispersity and the experimental conditions can be difficult to replicate consistently, leading to even larger variations between batches.

An alternative to this method is to form each particle individually using a microfluidic device, which will be described in detail in the next section. In general, droplets produced using this method are highly uniform in size. While this process is slower than the emulsion method, the monodispersity of the particles far outweighs the small production throughput for this study. Another benefit is that this system can be set up to produce particles continuously, which is almost always preferable to batch production. There are many configurations of droplet forming microfluidic devices currently in development, but most commercial options are prohibitively expensive. Instead, it was decided to construct a microfluidic device in-house using easily obtained and inexpensive materials.

In summary, the objectives of this study are 1) to develop a simple and inexpensive method to produce monodisperse polymer microparticles, 2) to examine the detachment behavior of microparticles in a microchannel, and 3) to characterize the adhesion forces acting between a microparticle and a microchannel for different material pairings.

2. THEORY AND MODEL

2.1 Creating Monodisperse Microparticles

To produce monodisperse polymer spheres, a microfluidic device was used to create single emulsion droplets of a monomer solution that could then be reacted to produce solid particles. The microfluidic device consists of a small capillary inserted down into a larger capillary. When in use, an oil-phase monomer solution is pumped through the inner capillary and an aqueous carrier solution is pumped through the outer capillary. This device works by creating droplets of the inner solution through flow-induced dripping, which is when a liquid is forced to form into droplets by a second immiscible fluid flowing parallel to it. As the inner fluid reaches the end of the inner capillary, it gathers until it eventually breaks off to form a droplet. The final diameter of the droplet (d_p) is determined by how much of the inner fluid can gather at the capillary tip before it breaks off and flows away. A schematic of the process for the device built in this study is shown in **Figure 2.1**.

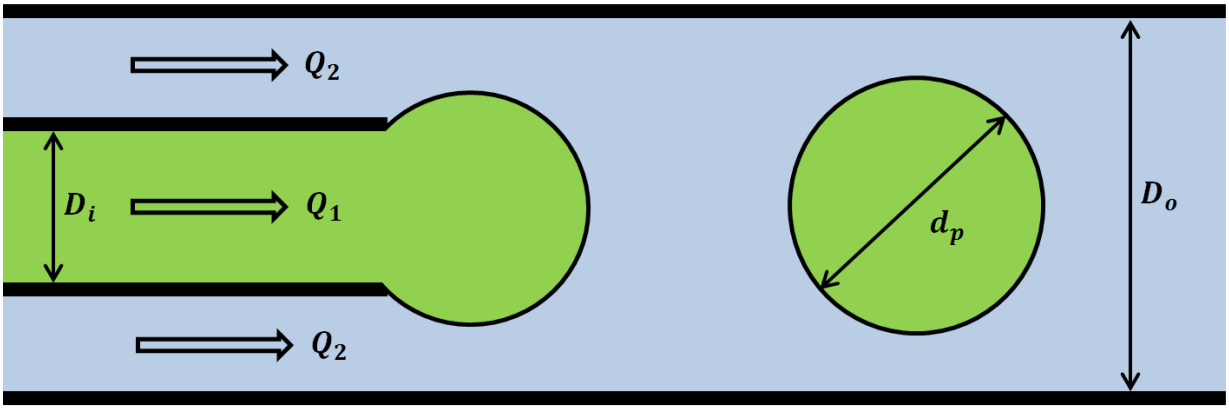

Figure 2.1: Schematic of the formation of single emulsion droplets in a microfluidic device, where Q_1 is the volumetric flow rate of the inner phase, Q_2 is the volumetric flow rate of the outer phase, D_i is the diameter of the inner channel, D_o is the diameter of the outer channel, and d_p is the diameter of the droplet formed by the flow-induced dripping.

The break-off point can be characterized by the capillary number (Ca), as expressed in **Equation 2.1** [6]:

$$Ca = \frac{F_{shear}}{F_{\gamma}} \tag{2.1}$$

where F_{shear} represents the viscous forces acting on the growing droplet and F_{γ} is the interfacial tension between the two immiscible liquids. The capillary number can be used to predict the break off point because it describes the balance of forces acting on the droplet. While the co-flowing outer fluid works to pull the droplet off the capillary tip through shear forces, the interfacial tension between the phases keeps the droplet attached. However, as the droplet grows, the shear forces begin to outweigh the interfacial forces and, at some critical capillary number, the droplet will break away from the inner capillary.

To determine the shear force acting on the droplet, a modified Stokes' drag force can be applied, as seen in **Equation 2.2** [6]:

$$F_{shear} = 3\pi\mu_2(d_p - D_i)(u_2 - u_1) \tag{2.2}$$

where μ_2 is the viscosity of the outer fluid, D_i is the diameter of the inner capillary, and u_1 and u_2 are the average velocities of the inner and outer fluids, respectively. The $d_p - D_i$ term in the equation reflects that the cross-section of the inner capillary shields part of the growing droplet from the shear forces of the outer fluid. The velocities used above are given in **Equation 2.3** and **Equation 2.4** [6].

$$u_1 = \frac{4Q_1}{\pi d_p^2} \tag{2.3}$$

$$u_2 = \frac{4Q_2}{\pi\left(D_o^2 - d_p^2\right)} \tag{2.4}$$

The force due to interfacial tension can be expressed as **Equation 2.5** [6]:

$$F_\gamma = \pi D_i \gamma_{1,2} \tag{2.5}$$

where $\gamma_{1,2}$ is the interfacial tension between the two fluids.

Unfortunately, these equations depend on many underlying assumptions that make them impractical and inaccurate for this system. For example, the equation for Stokes' drag force assumes that the droplet is rigid, while it is actually a flexible liquid. A fluid droplet experiences less drag than a rigid particle because it is able to flex. Another assumption is that the walls of the outer capillary have a negligible effect on the shear forces. Yet, these walls create a very restricted geometry, causing large velocity gradients and increasing the drag acting on the droplet [6].

Nevertheless, while the assumptions that govern these equations make calculations impractical for this system, the relationships can still be useful for predicting the effect a physical quantity will have on the size of the resultant droplets. For instance, as the volumetric flowrate of the outer phase is increased, the shear forces will also increase, causing droplets to break off sooner and resulting in smaller particles. The same can be said for increasing the viscosity of the outer phase or decreasing the volumetric flow rate of the inner phase. These relationships will be used to fine tune the size of the particles produced using the microfluidic device.

2.2 Detachment Behavior of a Microparticle in a Microchannel

To analyze the detachment behavior of individual particles in microfluidic flow, all of the forces acting on the particle must be accounted for. The geometry of this system can be modeled as a spherical solid lying on the bottom of a cylindrical tube and experiencing shear fluid flow. This sphere has a diameter with the same order of magnitude as the channel, so that the laminar flow profile is significantly altered as the fluid passes over the particle. A sketch of this system is shown in **Figure 2.2**. The vertical forces on the particle include gravity (F_G), buoyancy (F_B), lift (F_L), and adhesion (F_A) while the horizontal forces include friction (F_F) and drag (F_D). In the case where the particle may begin to roll, moments also act to rotate the particle: the moment induced by friction (M_F) and the moment caused by the effective drag of the fluid (M_{EffD}). However, for these moments to be applicable, it must first be confirmed that the particle undergoes detachment through rolling.

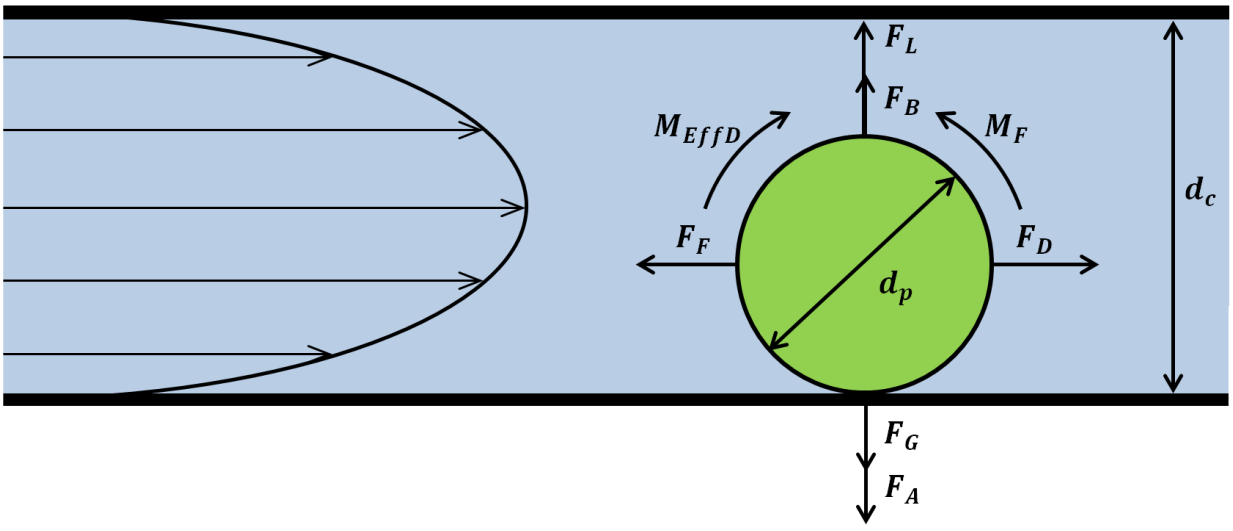

Figure 2.2: The forces and moments acting on a large particle in restricted, laminar flow.

2.2.1 Rolling Moment

In previous work, it has been shown that microparticle detachment from a wall due to fluid flow is induced by either a rolling or a sliding motion. Once the particle begins to move, it can lift off the bottom of the channel and become fully entrained in the fluid. Whether or not the lift off is caused by rolling or sliding can be determined by through the rolling moment (RM) [8]. The rolling moment is the ratio of the hydrodynamic rolling forces to the adhesion resting moment and can be calculated using **Equation 2.6**:

$$RM = \frac{F_D\left(1.399\ \frac{d_p}{2} - \alpha\right)}{(F_A + F_G - F_B - F_L)\frac{a_{eq}}{2}} \tag{2.6}$$

where d_p is the diameter of the particle, α is the deformation at the interface between the particle and the channel, and a_{eq} is the particle's contact diameter with the bottom of the channel. According to the literature, if the value of RM is greater than 1, rolling will occur; if not, motion will be induced through sliding [8]. The deformation can be calculated using **Equation 2.7**:

$$\alpha = \frac{d_{p,eff}}{2} - \left[\left(\frac{d_{p,eff}}{2}\right)^2 - \left(\frac{a_{eq}}{2}\right)^2\right]^{\frac{1}{2}} \tag{2.7}$$

where $d_{p,eff}$ is the effective diameter of the particle in the channel. The effective diameter of the particle accounts for the geometry of a sphere in contact with a surface. If the particle is sitting on a flat surface, the effective diameter is equal to the particle diameter. However, the particle in this system is in contact with the inside of a cylinder, which acts as an inverted sphere along its width and like a plane along its length. To account for this asymmetric geometry, the effective

diameters for both an inverted sphere and a plane were calculated and the average was taken as the effective diameter for this system. This is shown in the equations below:

$$d_{p,eff} = \frac{\left(d_{p,eff,sphere} + d_{p,eff,plane}\right)}{2} \tag{2.8}$$

$$d_{p,eff,sphere} = \left(\frac{1}{d_p} - \frac{1}{d_c}\right)^{-1} \tag{2.9}$$

$$d_{p,eff,plane} = d_p \tag{2.10}$$

where $d_{p,eff,sphere}$ is the effective diameter of a sphere in contact with an inverted sphere, $d_{p,eff,plane}$ is the effective diameter of a sphere in contact with a flat plane, d_p is the diameter of the particle, and d_c is the diameter of the channel.

Theoretically, a solid sphere should make contact with a solid surface at a single point. However, both the sphere and the surface experience some slight deformation at the point of contact, resulting in a larger contact area between the two surfaces. This area can be characterized with the contact diameter, which is defined in **Equation 2.12** according to the JKR theory [9].

$$a_{eq} = \left(\frac{6\pi W_A d_{p,eff}^2}{4K}\right)^{\frac{1}{3}} \tag{2.12}$$

In this equation, W_A is the work of adhesion and K is the composite Young's modulus, which is defined in **Equation 2.13** [9]**:**

$$K = \frac{4}{3(k_1 + k_2)} \tag{2.13}$$

where k_i is the elastic coefficient for the ith material, which is either the particle or the channel. This coefficient is a function of the material's Young's modulus of elasticity (E_i) and Poisson's ratio (ν_i), and is expressed in **Equation 2.14** [9].

$$k_i = \frac{1 - \nu_i^2}{E_i} \tag{2.14}$$

The work of adhesion is defined as the difference in surface energy caused by contact between the two solids, as expressed in **Equation 2.15**:

$$W_A = \gamma_1 + \gamma_2 - \gamma_{12} \tag{2.15}$$

where γ_i is the surface energy of the ith material and γ_{12} is the interfacial energy between the two [10]. While some values for γ_i are reported in the literature, most are only available for specific systems, usually while exposed to air or held in a vacuum. There is very little data available for systems exposed to water. Additionally, the aqueous fluid in this system contains a surfactant, which can significantly modify the surface energy of any material it comes into contact with. Therefore, the work of adhesion cannot be calculated through readily available material properties and must be measured experimentally.

2.2.2 Moment Balance on a Rolling Particle

For all experiments conducted in this study, particle motion is induced through rolling, as will be verified in later sections. Therefore, a balance of moments is more appropriate than a balance of forces for this system. As seen in **Figure 2.2**, there are two moments acting on the particle: the moment induced by friction (M_F) and the moment caused by the effective drag of the fluid (M_{EffD}). For rolling to take place solely through fluid flow, these moments must equal

each other at the point where the particle begins to roll [7]. The effective drag moment is expressed in **Equation 2.16** [9]:

$$M_{EffD} = 1.74 \left(\frac{d_p}{2}\right) F_D \tag{2.16}$$

where d_p is the particle diameter and F_D is the drag force. The factor of 1.74 in **Equation 2.16** accounts for the eccentricity of the drag force [11]. The other moment acting on the particle is induced by the frictional force acting parallel to the surface of the sphere that is in contact with the channel and can be calculated using **Equation 2.17** [7]

$$M_F \leq a_{eq}(F_G + F_A - F_L - F_B) \tag{2.17}$$

where $a_{eq}$is the contact diameter defined in **Equation 2.12**. When combined together, the moment balance on the particle at the point of detachment is expressed as **Equation 2.18**.

$$1.74 \left(\frac{d_p}{2}\right) F_D = a_{eq}(F_G + F_A - F_L - F_B) \tag{2.18}$$

This balance allows the forces that are more difficult to calculate, such as adhesion, to be found as a function of the other forces.

2.2.3 Forces Acting on the Particle

Some of the forces acting on the particle are already well defined for general systems and can be determined simply from the material properties of the system. The forces due to both gravity and buoyancy fall into this category and are defined in **Equation 2.19** and **Equation 2.20**, respectively:

$$F_G = g\ \rho_p V_p = \frac{4\pi g \rho_p}{3}\left(\frac{d_p}{2}\right)^3 \tag{2.19}$$

$$F_B = g\ \rho_f V_p = \frac{4\pi g \rho_f}{3}\left(\frac{d_p}{2}\right)^3 \tag{2.20}$$

where g is the acceleration due to gravity, V_p is the volume of the particle, ρ_p is the density of the particle, and ρ_f is the density of the fluid being displaced by the particle.

On the other hand, drag and lift forces are far more difficult to calculate. The theoretical equations that already exist in the literature make several assumptions that are not valid for the system defined above. In the case of drag forces, Stoke's Law, as seen in **Equation 2.21**, is one of the most well-known methods for calculating the drag on a small sphere moving freely through a viscous liquid [9]:

$$F_D = 3\pi\mu d_p u \tag{2.21}$$

where μ is the dynamic viscosity of the fluid and u is the fluid's velocity relative to the sphere. It has also been found that the presence of a wall increases the drag and that multiplying the drag force by a correction factor of 1.7009 is necessary [11]. However, the restricted geometry of this particular system presents a significant problem because the particle is large enough to obstruct flow, causing the fluid's velocity to increase as it passes over the particle. The equation above assumes that the fluid velocity around the particle is a constant value that is unaffected by the presence of the particle, which is not valid for this system. A similar problem arises when attempting to calculate lift force. For a particle attached to a wall exposed to a simple shear flow, the mean lift force can be expressed as **Equation 2.22** [12]:

$$F_L = 9.22\ \frac{u^4 \rho_f^3}{\mu^2}\left(\frac{d_p}{2}\right)^4 \tag{2.22}$$

where u is the velocity of the fluid, ρ_f is the density of the fluid, and μ is the dynamic viscosity of the fluid. Again, this theory does not account for the confined geometry of the system or the significant pressure gradients generated as the fluid accelerates over the particle. These pressure gradients alter the amount of lift acting on the particle, making this equation unusable for the system.

Because this confined geometry creates many problems that have not been addressed in the literature, traditional equations cannot be used to calculate the drag and lift forces. Instead, a computational fluid dynamics (CFD) simulation was made to model the flow of water through a small channel with a spherical obstruction fixed to the bottom. This simulation was created using the COMSOL Multiphysics® 5.1 software (COMSOL Inc., Burlington, MA). Using this simulation, the stresses on the spherical obstruction can be approximated. The horizontal stress corresponds to the drag force and the vertical stress to the lift force. The details of this model are described in **Appendix A**.

The last force that appears in the moment balance is the adhesion force. In past studies, this force has been attributed solely to van der Waals attractions [7]. An expression for the van der Waals forces ($F_{A_{van\ der\ Waals}}$) between a sphere and a flat surface is provided in **Equation 2.23** [13]:

$$F_{A_{van\ der\ Waals}} = \frac{A_H d_p}{12 s^2} \tag{2.23}$$

where A_H is the Hamaker constant and s is the spacing between the sphere and the flat surface. For a glass particle in a PDMS channel, appropriate values for the Hamaker constant and the

spacing are $A_H = 10^{-19}J$ and $s = 8 \times 10^{-8}m$, making the van der Waals forces exclusively dependent on particle diameter [13]. However, the assumption that the only adhesion forces present on the particle are van der Waals forces neglects other important factors, such as surface chemistry interactions and electrostatic effects. It also does not consider the elastic Hertzian forces pushing the particle away from the channel wall. A better model would be to use the pull-off force as defined in the JKR theory, as shown in **Equation 2.24** [9]:

$$F_{A_{JKR}} = 1.5\pi W_A \left(\frac{d_{p,eff}}{2}\right) \tag{2.24}$$

where W_A is the work of adhesion and $d_{p,eff}$ is the effective particle diameter. This adhesion force is considered to be the difference between the adhesion and Hertzian forces, accounting for both the elastic forces and general adhesion, which includes van der Waals forces. It also relates the adhesion force to the work of adhesion, which is constant for a given material pairing. While this parameter must be determined experimentally, it provides a convenient way to characterize adhesion and makes this analysis applicable to any pairing of particle and channel materials. One of the primary goals of this study will be to determine this work of adhesion for several different material pairings and examine the adhesive forces present.

All of the relationships presented here work together to associate the drag force, lift force, and work of adhesion to one another. As stated previously, the drag and lift forces can be determined through experimental results, allowing the work of adhesion to be calculated.

3. EQUIPMENT, MATERIALS, AND METHODS

3.1 Synthesizing Polymer Microparticles

3.1.1 Constructing the Double Emulsion Droplet-Forming Microfluidic Device

With the initial intention of producing double emulsion droplets for synthesis into liquid-filled polymer spheres, the first microfluidic design was modeled from a device created by Nurumbetov et al. [14]. This original design consisted of larger glass capillary with a 1 mm diameter hole drilled into it midway down its length. A smaller capillary was inserted into the hole, extending halfway into the larger capillary's diameter, and glued into place with epoxy glue. Tubing was connected to the exposed end of the smaller capillary and a 30 gauge needle with a right angle bent into it midway down its length was inserted through the wall of the tubing and down into the smaller capillary. A schematic of this design can be seen in **Figure 3.1** and the details for all of these materials can be found in **Appendix B**. Tubing was then connected to the smaller and larger capillaries, and barbed adapters facilitated the attachment of syringes to each capillary and the needle. In this configuration, the aqueous inner phase, the oil phase monomer solution, and the aqueous outer phase were introduced through the needle, small capillary, and large capillary, respectively.

To create the liquid core of the capsule, the inner phase was introduced through the needle, which formed small immiscible droplets in the oil phase liquid flowing through the smaller capillary. The polymer shell was then formed by depositing droplets of the monomer

solution into the viscous outer phase flowing through the larger capillary. Ideally, each monomer droplet should contain one inner phase droplet of its own. Once these double emulsion droplets were formed, the entire solution could be exposed to UV light. If an appropriate photoinitiator was included in the monomer solution, the oil phase monomer solution would polymerize and solid polymer shells containing liquid cores would be formed.

While the behavior of polymer capsules provided the original inspiration for this project, considerable problems arose while attempting to synthesize them. These difficulties will be discussed in detail in Section 4.1.1. However, due to these complications and time constraints, it was decided to modify the scope of the project to focus on the production and behavior of solid polymer spheres produced from single-emulsion droplets.

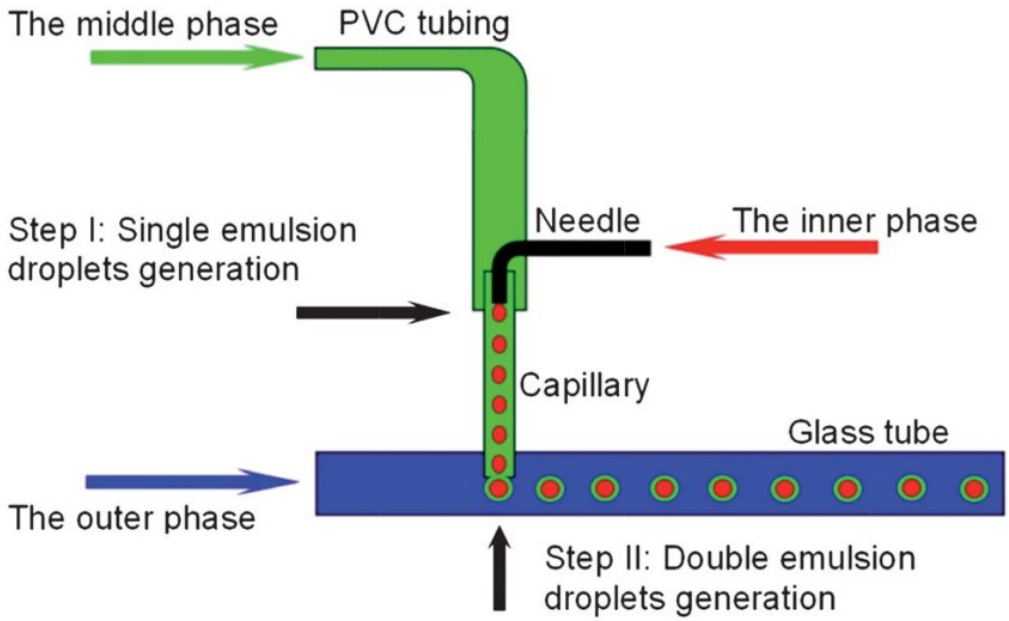

Figure 3.1: A schematic representation of the double-emulsion droplet generating microfluidic device developed by Nurumbetov et al. [14].

3.1.2 Constructing the Single Emulsion Droplet-Forming Microfluidic Device

Using the same components as the double emulsion configuration, a single-emulsion variant of the microfluidic device was developed. This device consisted of a single small capillary with one end connected to the tubing and the other exposed. A long 30 gauge needle was modified by bending it into a right angle approximately 30 mm from its tip. It was then incorporated into the device by puncturing a small hole in the tubing close to the connection with the capillary and inserting the needle up to the bend. An image of the device can be seen in **Figure 3.2** and the details for these materials can be found in **Appendix B**.

A female Luer adapter was connected to the end of the tubing attached to the capillary, allowing it to connect to a 1000 μL syringe, while the needle was connected directly to a 500 μL syringe. The syringes were independently controlled using two separate syringe pumps. Each pump was programmed with the inner diameter of the syringe and the desired volumetric flow rate for each solution. A picture of the device connected to the syringe system can be seen in **Figure 3.3**.

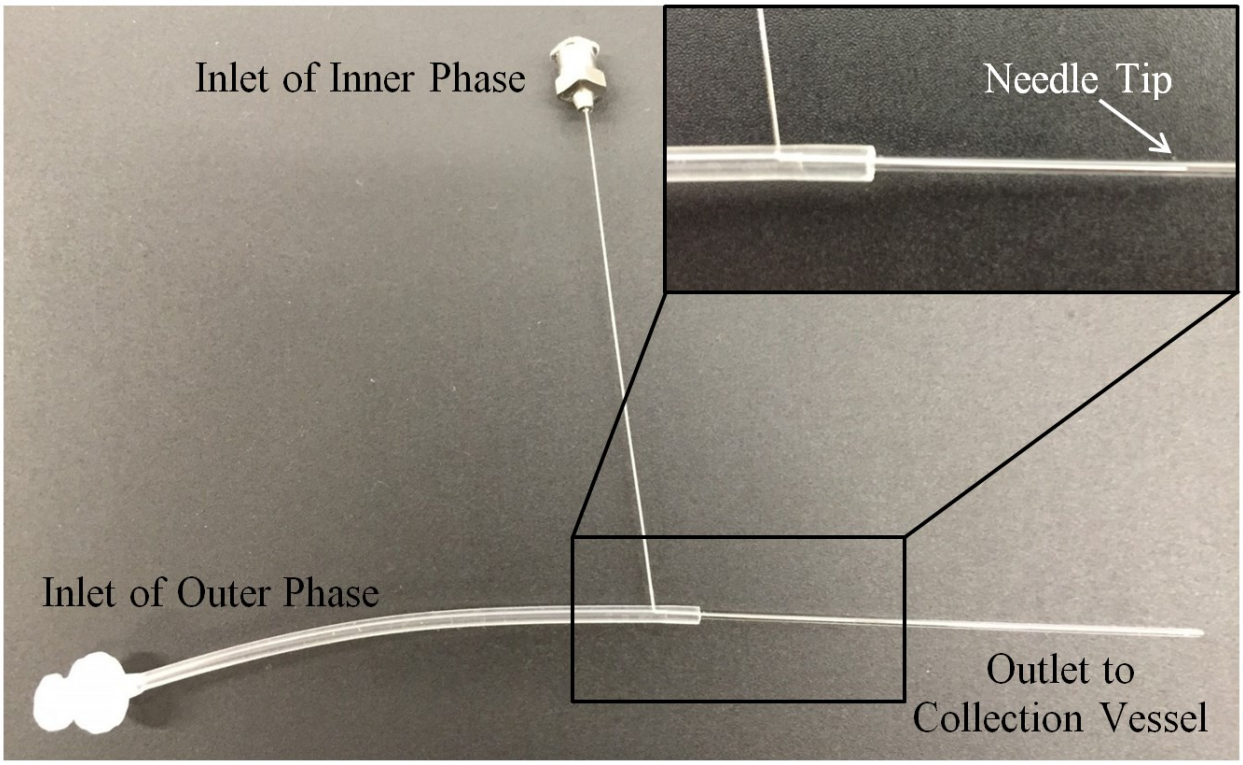

Figure 3.2: A close up of the simplified microfluidic device for the generation of single-emulsion droplets.

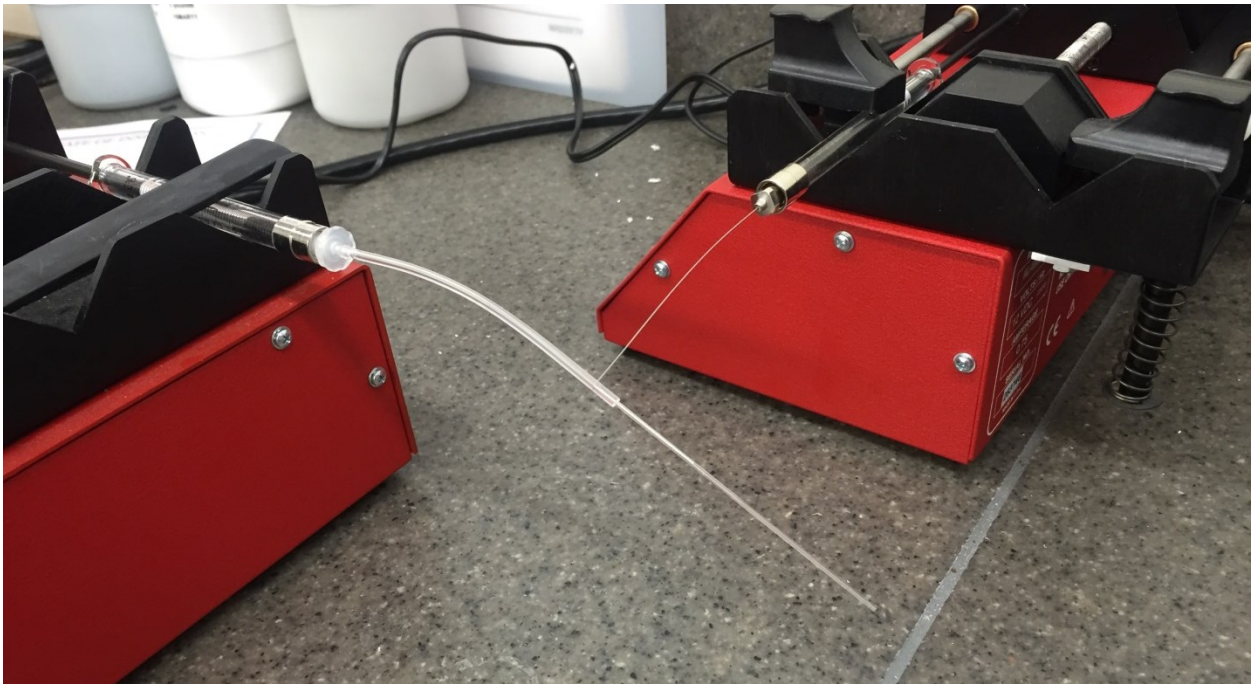

Figure 3.3: The simplified microfluidic device connected to the syringe pumps.

3.1.3 Solutions Used in Creating Single-Emulsion Droplets

To create the droplets, both an oil-phase monomer solution and an aqueous outer phase were used. Two different kinds of polymer microparticles were made using this device, each requiring their own monomer and carrier solutions. The first, poly(isobornyl acrylate), was chosen because it has been extensively discussed in the literature as a model system for particle synthesis through microfluidic emulsion techniques. This is because it is highly immiscible in water and easily synthesized through UV exposure [6,14]. However, because it is not a common polymer, it would not be useful as a candidate in the microparticle detachment experiments. Instead, it is valuable only as a sample system to assess the abilities of the single-emulsion microfluidic device. The second polymer system, poly(methyl methacrylate), was chosen because it is a very common polymer and has different physical properties than glass, making it an ideal candidate for comparison against glass in microfluidic flow behavior.

To make the poly(isobornyl acrylate), PIBA, microparticles, the oil-phase solution contained primarily the monomer, isobornyl acrylate (IBA), with 1 wt.% of 2,2-dimethoxy-2-phenylacetophenone (DMPA) added as a photoinitiator. The solution was stirred until the DMPA dissolved and was stored in a dark drawer until use. The carrier phase for this system was a 5 wt.% aqueous solution of poly(vinyl alcohol), PVA. For each 10 mL batch, 0.51g of PVA was added to deionized water and stirred vigorously over low heat until it dissolved completely. The resulting solution was stored in a dark drawer until use [14]. Details for these chemicals can be found in **Appendix B**.

To make the poly(methyl methacrylate), PMMA microparticles, a more complicated monomer solution was necessary. This solution contained methyl methacrylate (MMA) as the monomer, ethylene glycol dimethacrylate (EGDMA) as an aid in the free radical copolymer crosslinking reaction, glycidyl methacrylate (GMA) as a crosslinking agent, and 2-methyl-4′-(methylthio)-2-morpholinopropiophenone (MTMP) as the photoinitiator. The composition of this solution was 87% w/v MMA, 5% w/v MTMP, 5% w/v EGDMA, and 3% w/v GMA. Once all of the components were combined, the solution was allowed to stir until everything was dissolved and it was stored under refrigeration until use. The carrier phase for this system was a 2% w/v aqueous solution of methyl cellulose (MC). This material has a lower critical solution temperature, meaning that MC is readily soluble in water below 40˚C, but will precipitate out of solution at elevated temperatures. However, preparing solutions of MC in cold water can be difficult because a gel layer will form on the surface of the powder, slowing the diffusion of water into the remainder of the solid particles. Instead, it is best to mix the MC into hot water and disperse the particles first, then cool the solution until it dissolves. Therefore, each solution was made by stirring 0.204 g of MC into 10 mL of 50˚C deionized water. Once it was evenly dispersed, the solutions were immersed in an ice bath to dissolve the MC and the solutions were stored in a drawer until use [6]. Details for these chemicals can be found in **Appendix B**.

3.1.4 Creating Solid Polymer Spheres Using the Microfluidic Device

The first step to preparing the device was to fill the syringes and insert them into the syringe pump. The smaller, 500 μL, syringe was filled with the monomer solution and installed into the single syringe pump while the larger, 1000 μL, syringe was filled with the appropriate

carrier solution and mounted into the larger, sextuple syringe pump. Each pump was programmed with the syringe's inner diameter and the desired volumetric flowrate. Next, the Luer lock fittings on the microfluidic device were connected to the syringes; the needle was attached to the smaller syringe while the tubing attached to the capillary was connected to the larger syringe. Both syringe pumps were then turned on and the solutions were allowed to fill the device completely, ensuring that all air pockets or bubbles were removed.

Once these steps were completed, droplets could be generated. To start a production run, the carrier solution was allowed to flow into a waste collection vessel until all traces of the monomer solution were cleared from the capillary. Next, a 20 mL glass collection vial containing a small amount of the carrier solution was placed over the open end of the device, submerging the end of the capillary completely in the solution. This allowed the droplets generated in the device to flow smoothly into the collection vessel, minimizing the risk of damaging the droplets before the polymerizing reaction could occur. Then, with the carrier solution already flowing into the collection vessel, the syringe pump connected to the monomer solution was started. As the monomer solution flowed through the needle into the much more viscous carrier solution, small droplets of the immiscible monomer solution were formed at the junction of the co-flowing solutions. These droplets were carried into the collection vessel, where they floated for the remainder of the trial. Once enough droplets were made, the collection vial was removed and set aside and a waste collection vessel was placed over the open end of the capillary. At that point, the monomer solution was turned off and the carrier solution was allowed to flow until the remainder of the monomer droplets were removed from the channel.

As soon as the pumping was stopped, the collection vial was placed into a UV light exposure system to initiate the polymerization reaction. As the particles were exposed to the UV light, observations in density differences were used to determine when the reaction reached completion For the poly(isobornyl acrylate) particles, 5 minutes was more than sufficient to complete the reaction. For the poly(methyl methacrylate) particles, 10 minutes of UV exposure was required. When the reaction was complete, the solid spheres could be moved and handled without damage. At this point, several of the particles were pipetted onto a sample dish and placed under the microscope for size determination. Using the "3-point circle" measurement tool in the Stream Imaging Software (Olympus Corp., Waltham, MA) the diameter of each sphere was determined and the average and standard deviation were recorded for the sample.

As mentioned previously, the poly(isobornyl acrylate) particles were only used to assess the capabilities of the single-emulsion microfluidic device. However, the poly(methyl methacrylate) particles were made with the intention of using them in further testing. In order to prepare these particles for microchannel detachment testing, several of the particles from each trial were pipetted into new 20 mL glass vials containing approximately 10 mL of the surfactant solution used in the microchannel testing. They were then allowed to stir in the shaker incubator at 200 rpm for 2 hours to wash the viscous carrier solution off of the particles.

3.2 Microparticle Detachment Behavior in Microchannels

3.2.1 Preparing the Microchannels

The PDMS microchannels were made using the Sylgard® 184 Silicone Elastomer kit. Each PDMS mold was a topless rectangular box 7.5 cm long, 5.5 cm wide, and 2.5 cm tall. An image of this assembly can be found in **Appendix B**. The two shorter edges were separate pieces that could be disconnected to make the removal of the PDMS easier. In each of the two longer sides, three aligned holes were drilled through the wall of the mold. These holes were small enough for a needle to fit snugly through and were aligned in such a way that three needles could be suspended in parallel across the rectangular mold approximately 1 cm above the bottom. For this project, three 25 gauge needles were inserted into the mold. At this point, a non-stick spray was applied to the assembled mold to prevent the PDMS from sticking too firmly. However, this spray was found to increase the surface roughness of the final microchannels, as investigated in **Appendix C**, so it was not used during the production of the microchannels used in the particle detachment testing. Once the mold was prepared, the Sylgard® 184 Silicone Elastomer base and curing agent were mixed in a 10:1 ratio. The mixture was stirred gently for about 5 minutes, taking care to both evenly distribute the curing agent within the base and avoid creating any bubbles. Once it was well mixed, the elastomer was poured gently into the mold, to a depth slightly above the suspended needles. If possible, any bubbles were removed or shifted away from the needles in the mold and the filled container was allowed to sit in the fume hood for 36 to 48 hours.

Once the PDMS solidified in the mold, the needles were very slowly removed, creating microchannels in the hollow spaces the needles had occupied. If any pieces of PDMS dislodged from the channel during this process, a smaller 30 gauge needle was inserted to carefully remove the obstruction without harming the rest of the channel. Once the channels were released, the detachable ends of the mold were separated and the entire block of PDMS was removed from the mold. After careful examination of the microchannels under the microscope to make sure the inner surface was smooth and unmarred, the channels were marked as acceptable for microparticle testing. To ensure the particle only experienced laminar flow, a length of 40 channel diameters (approximately 2 cm) was marked on both ends of the channel in order to avoid end effects. A picture of the completed PDMS microchannels with the ends marked off can be seen in **Figure 3.4**. The details for all of these materials can be found in **Appendix B**.

For the glass microchannel, a small capillary with an inner diameter of 500 μm was fitted with a short length of tubing on one end and was taped to a microscope slide for easier handling. Again, both ends were marked off to avoid interference by end effects.

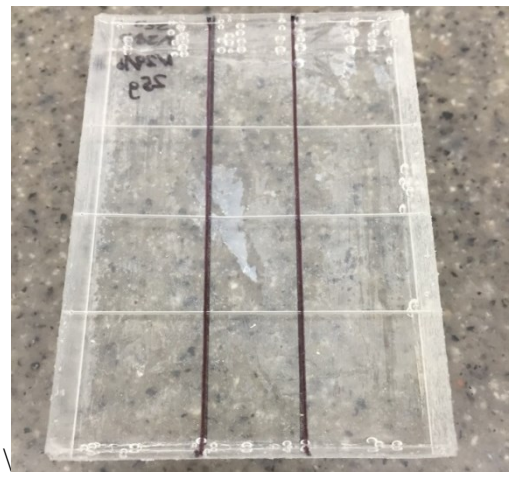

Figure 3.4: A set of three completed PDMS microchannels. The region marked off in the center is where all particle trials will take place to avoid the end effects on the flow profile.

3.2.2 Microparticle Detachment Experiments

The goal of these experiments was to record the fluid velocity required to detach a settled microparticle from the wall of a microchannel. An aqueous solution containing a surfactant was chosen to move the particles in order to reduce the effect of adhesion [7]. While the goal of the study is to examine the adhesive forces, the particles were too difficult to move using the available equipment without the aid of a surfactant. Tween 80 was chosen as an appropriate surfactant and a low concentration of 0.15 g/L was sufficient to allow the particles to move in an appropriate range of flow rates without noticeably altering the properties of the solution. Therefore, the properties of this solution were assumed to be the same as deionized water.

To prepare the microchannel for a trial, a syringe full of the Tween 80 solution was installed into the syringe pump and attached to one end of the channel. This syringe either held 5000 μL or 1000 μL, depending on the precision required for the trial. For the PDMS channel trials, a length of tubing with a male Luer connector on one end and a female connector on the other was attached to a small 25 gauge needle and the full syringe, respectively. The small needle was then inserted into one end of a PDMS channel, which provided a tight enough seal to allow low pressure flow rates through the channel. For the glass channel trials, the syringe was attached directly to a female Luer adapter connected to the length of tubing already attached to the capillary. Once the syringe was connected, the channel was rinsed with the Tween 80 solution to ensure that all air bubbles and any small particulates were removed. The full channel was then inspected under the microscope for any aberrations and set aside.

Next, several particles in the desired size range were submerged in a small amount of the Tween 80 solution in a glass sample dish. The particles were either pre-purchased glass particles with specified size ranges or the PMMA particles made as described previously. The dish was placed under the microscope and a particle with the desired diameter was found using the Stream Essentials software connected to the microscope. Once the outer diameter of the chosen particle was found and recorded, a small needle was used to isolate the particle in the microscope's field of view. To transfer the particle from the sample dish to the microchannel, a 100 μL syringe with a short 25 gauge needle attached was used to suck up the isolated particle and remove it from the Tween 80 solution. Particles smaller than 260μm could fit inside the 25 gauge needle, and for larger particles, suction was maintained as the particle was lifted up and out of the solution, which kept the particle attached to the tip of the needle until it could be placed into the channel.

Once the particle was picked up and ready to be placed into the channel, the dish was removed from the microscope platform and replaced with the microchannel. The tip of the 25 gauge needle containing the particle was then inserted into the end of the channel and the particle was injected with the aid of the microscope. Once the depositing needle was removed, a long 30 gauge needle was used to push the particle deeper into the channel, to the far end of the center zone marked out for trials. Once the particle was in the correct location, the 30 gauge needle was removed and the end of the channel was exposed to more of the Tween 80 solution in order to minimize the effect of pressure gradients.

Once the microparticle was in place and the channel was fully prepared, attempts to dislodge the particle could begin. First, the syringe pump was set to a flow rate significantly

higher than the detachment velocity to roll the particle to a fresh position. Next, the particle was allowed to fully settle to the bottom of the channel. As described in **Appendix D**, the settling time was calculated for each set of particles and at least doubled. Even for the denser particles, a minimum settling time of one minute was used to make sure that all particles were fully seated on the bottom of the channel. After this settling time, the syringe pump was set to a considerably lower flow rate than that needed for detachment and the laminar flow profile was allowed to develop over a minute. Once the flow profile was established, the flow rate was increased incrementally until the particle dislodged from its position in the channel. After a baseline detachment rate was established, these increments were decreased as the flow rate approached dislodgement to ensure a more accurate measurement. For these experiments, detachment was defined as the point at which the particle rolled more than one particle diameter from its original location, which was monitored using the microscope's software.

Once the particle was dislodged, it was shifted to a new location and allowed to resettle. The process was then repeated until at least seven detachment rates were recorded for the particle. After the flow rates were recorded, a high flow rate was used to force the particle out of the channel, where it was subsequently discarded. The process was then repeated for additional particles. To disassemble the system, the syringe was detached and emptied. Air was then forced through the channel and all attached tubing, clearing the water from the system and allowing the channel to be stored safely. The details for all the materials and equipment used in these experiments can be found in **Appendix B**.

4. RESULTS AND DISCUSSION

4.1 Production of Monodisperse Polymer Microparticles

4.1.1 Attempts to Produce Liquid-Filled Polymer Spheres from Double Emulsion Droplets

As mentioned previously, the original goal of this project was to study the behavior of liquid-filled polymer spheres. However, once the microfluidic device was constructed following the design proposed by Nurumbetov et al., there was significant difficulty in producing double emulsion droplets [14]. Larger single emulsion droplets of the oil phase monomer solution were able to be created consistently, but problems arose when trying to put the smaller aqueous droplets inside the oil phase droplets to create the double emulsion. A recurring issue was noticed that, as the inner phase solution exited the needle, it formed a solid stream along the side of the smaller capillary, flowing alongside the monomer solution rather than emulsifying into droplets. It was believed that this problem was due to either an issue with the ratio of flow rates between the inner and middle phases or a problem with the geometry, where the needle would rest against the wall rather than stay suspended in the center of the smaller capillary. However, while various attempts were made to rectify these problems, such as altering the inner phase flow rate from the recommended levels and building a support system for the microfluidic device, the issue continued to prevent the production of double emulsion droplets. Eventually, the production of liquid-filled polymer spheres was abandoned for the sake of time constraints. As

an alternative, a simpler version of the device was constructed using many of the same materials to successfully produce single emulsion droplets.

4.1.2 Production of Poly(Isobornyl Acrylate) Microparticles

Following the construction of the single emulsion microfluidic device, trials were first run to produce poly(isobornyl acrylate), PIBA, particles to confirm that the device functioned as intended. The desired size range for d_p was between 100 and 500 μm and appropriate flow rate pairings were found through trial and error. A plot of the diameters of the particles (d_p) produced through this process can be seen in **Figure 4.1**. Full details for these results can be found in **Table E.1** in **Appendix E**.

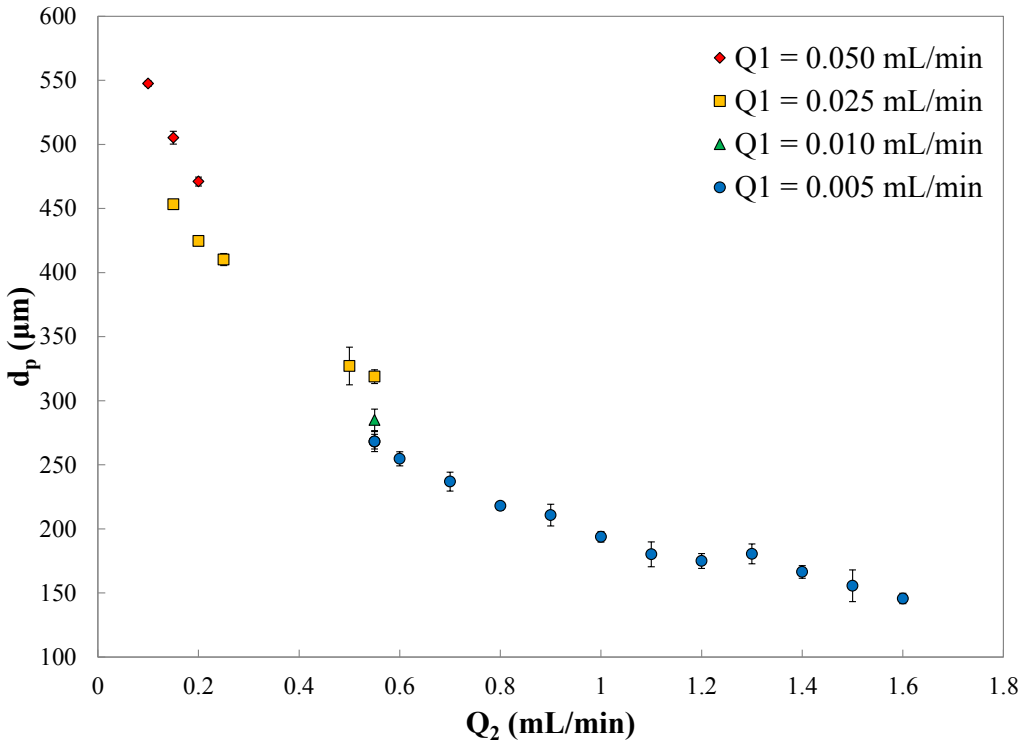

Figure 4.1: The relationship between the IBA solution and PVA solution flow rates and the diameter of the poly(isobornyl acrylate) particle produced. In this case, the flow rate of the IBA solution is given by Q_1 and the flow rate of the PVA solution is given by Q_2.

In this figure, it can be observed that small changes in the inner phase flow rate (Q_1) caused relatively dramatic shifts in d_p. For example, the drop from $Q_1 = 0.050\ mL/min$ to $Q_1 = 0.025\ mL/min$ caused a $50\ \mu m$ decrease in particle diameter. On the other hand, the outer phase flow rate (Q_2) could be changed by much larger increments and to cause much smaller modifications to d_p. For smaller particles, an increase in Q_2 of $0.1\ mL/min$ decreased d_p by between $5\ \mu m$ and $20\ \mu m$. This relationship between Q_1, Q_2, and d_p is highly useful for tuning the size of the produced particles. For future production, Q_1 can be used to set the desired overall size range of the particles produced in the device while Q_2 will be responsible for fine tuning the particle diameter to the desired quantity. However, this behavior is highly dependent on the particular pair of solutions being used. With solutions of different viscosities and interfacial tensions than the IBA and PVA solutions, the same drop in Q_1 or Q_2 will not cause the same change in particle diameter. Therefore, a general calibration curve for this device is not possible to produce experimentally. Instead, each pair of solutions will need to have their own calibration curve generated. Work has been done in this field to find a method of predicting droplet diameters by accounting for the capillary number, but further development is needed before this method will become practical to apply to general systems [6]. Overall, the production of PIBA particles displayed a general trend that, as Q_2increases, d_p decreases sharply and then begins to level off. This leveling off point can be adjusted by changing Q_1, but each value of Q_1 will only have a limited range of particle diameters possible.

The production of PIBA particles also demonstrated the precision of this microfluidic device. On average, each sample had a standard deviation of approximately $\pm 2.6\%$ of the particle's diameter. As a comparison, precision grade, commercially available glass

microspheres with similar particle diameters to the ones in this study can have size ranges of 30 μm to 50 μm in a single batch, which corresponds to approximately 8% to 9% of the batch's average particle diameter [15]. The particles produced using this microfluidic device are far more precise than the similar commercially available particles and can be considered monodisperse.

4.1.3 Production of Poly(Methyl Methacrylate) Microparticles

Once the initial analysis of the device was completed with the PIBA particles, poly(methyl methacrylate), PMMA, particles were created for use in microparticle flow analysis. To meet the desired d_p between 100 and 500 μm, a flow rate of 0.01 mL/min was chosen for Q_1. A plot of the particles produced by varying Q_2 is provided in **Figure 4.2**. Full details for these results can be found in **Table E.2** in **Appendix E**.

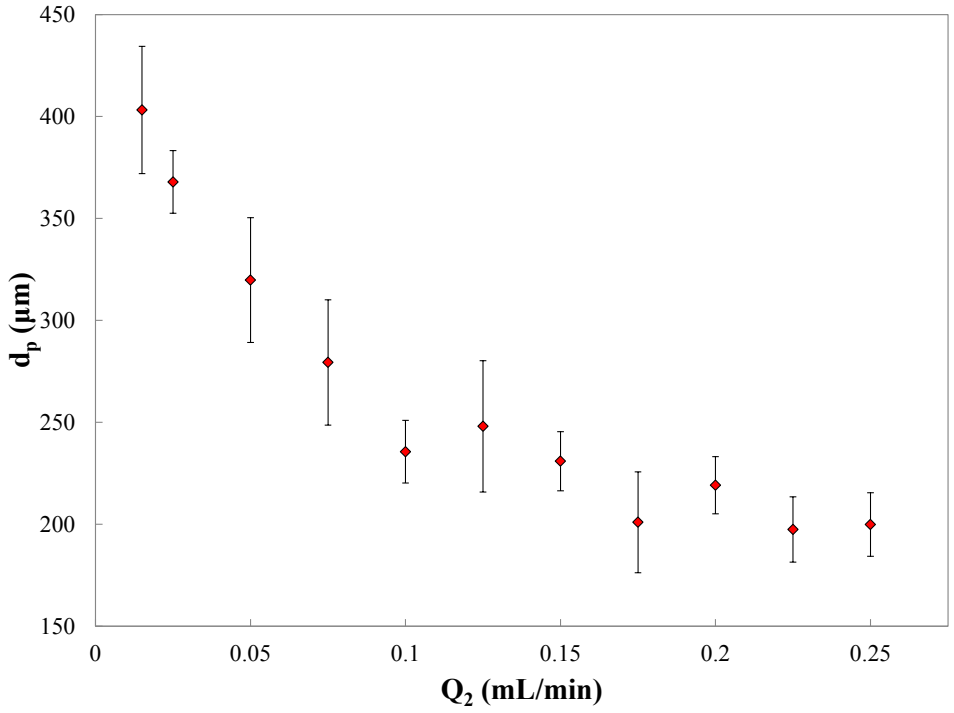

Figure 4.2: The relationship between Q_2 and d_p with a fixed value of $Q_1 = 0.01\, mL/min$ for the production of poly(methyl methacrylate) particles.

From this figure, it can be seen that the same general trend observed for the PIBA particles is also present for the production of PMMA particles: as Q_2 increases, d_p decreases sharply before leveling off. However, the values of Q_2 corresponding to a particle diameter are significantly lower for this system. For example, to produce a particle with $d_p \approx 280\ \mu m$ and $Q_1 = 0.010\ mL/min$, the PIBA system required $Q_2 = 0.55\ mL/min$ while the PMMA system only needed $Q_2 = 0.075\ mL/min$. This large discrepancy can be attributed to the difference in viscosity of the outer phase solutions. While both inner phase solutions had relatively low viscosities, the PVA solution used as the outer phase in the IBA system had a viscosity of $0.0381 \pm 0.0002\ Pa \cdot s$ while the MC solution used in the PMMA system had a viscosity of $0.2278 \pm 0.0301\ Pa \cdot s$. A higher viscosity solution will produce more shear force on a growing droplet as it flows past it, causing the droplet to break away from the tip of the needle at lower flow rates. This behavior makes viscous solutions more favorable for producing smaller particles and also reduces the amount of carrier solution required during particle production.

However, while this system can produce smaller PMMA particles more easily, the size range of the produced particles has more variability. The average standard deviation of the particles produced is approximately $\pm 8.4\%$ of the particle's diameter. While this is a significantly wider range than that of the PIBA particles, it is similar to the uncertainty of the precision grade commercial options, allowing them to also be classified as monodisperse.

4.2 Detachment Behavior of a Microparticle in a Microchannel

4.2.1 Experimental Detachment Velocities

Detachment experiments were conducted on four different pairings of particle and channel materials. These four combinations were glass particles in PDMS channels, glass particles in glass channels, PMMA particles in PDMS channels, and PMMA particles in glass channels. For each combination, particles in the size range between $150\ \mu m$ and $450\ \mu m$ in diameter were studied and the volumetric flow rate that induced particle detachment was recorded. Seven detachment data points were recorded for each particle; these experimental results can be seen in **Appendix F**. Because the PDMS channel had a diameter of $d_c = 510\ \mu m$ and the glass channel had a diameter of $d_c = 500\ \mu m$, the results were converted to alternate quantities to remove the influence of the channel diameter. The particle diameter (d_p) was converted into the ratio between the particle diameter and the channel diameter (d_p/d_c) and the volumetric flow rate of the fluid (Q) was converted into the inlet velocity of the fluid (u). This conversion allows results between trials in different channels to be compared to one another, as in **Figure 4.3**.

As seen in the figure, the glass particles required a significantly higher fluid velocity to induce detachment. This can be attributed to the density difference between glass and PMMA: the glass particles have a density of $\rho_{glass} = 2.54\ g/mL$ while the PMMA particles have a density of $\rho_{PMMA} = 1.18\ g/mL$. Because the PMMA particles have a lower density, gravity does not act as strongly on them, allowing them to move more easily.

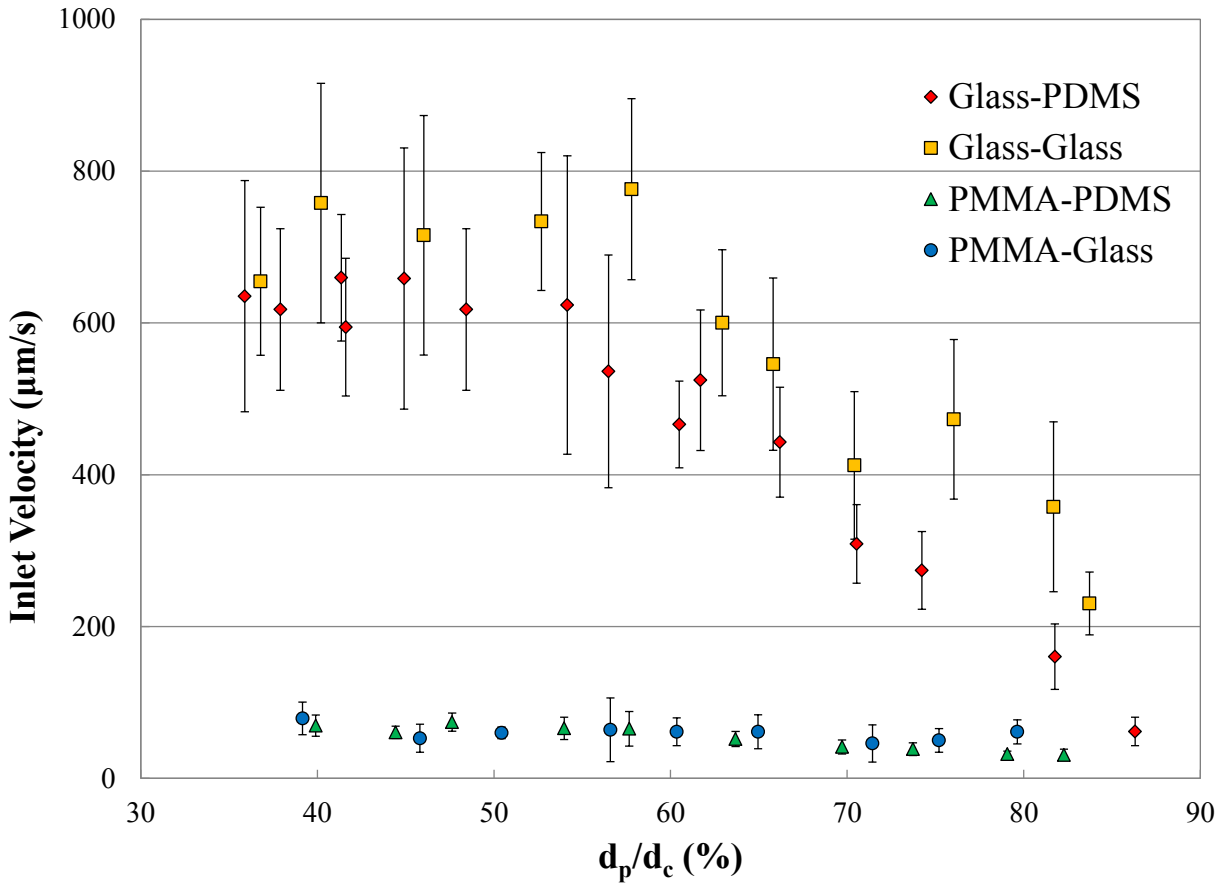

Figure 4.3: A comparison of the experimental results for microparticle detachment in a microchannel, where d_p is the diameter of the particle and d_c is the diameter of the channel. In the legend, the first material corresponds to the particle and the second material corresponds to the channel.

Another observation that can be made from this figure is that, at some diameter ratio between 50% and 60%, the detachment velocity starts to decrease. This point is where the particle becomes so large that it starts to block a significant portion of the microchannel and the flow exerts more force on the particle. While it can only be seen clearly for the glass particles in this figure, a comparison of only the PMMA particles, as seen in **Figure 4.4**, displays the same trend for the PMMA particles in the PDMS channel. For the PMMA particles in the glass channel, the trend is obscured by experimental error. However, because the other three data sets

exhibit the same behavior, it is reasonable to assume that this material pairing would behave similarly if these experiments were repeated using a more precise testing method.

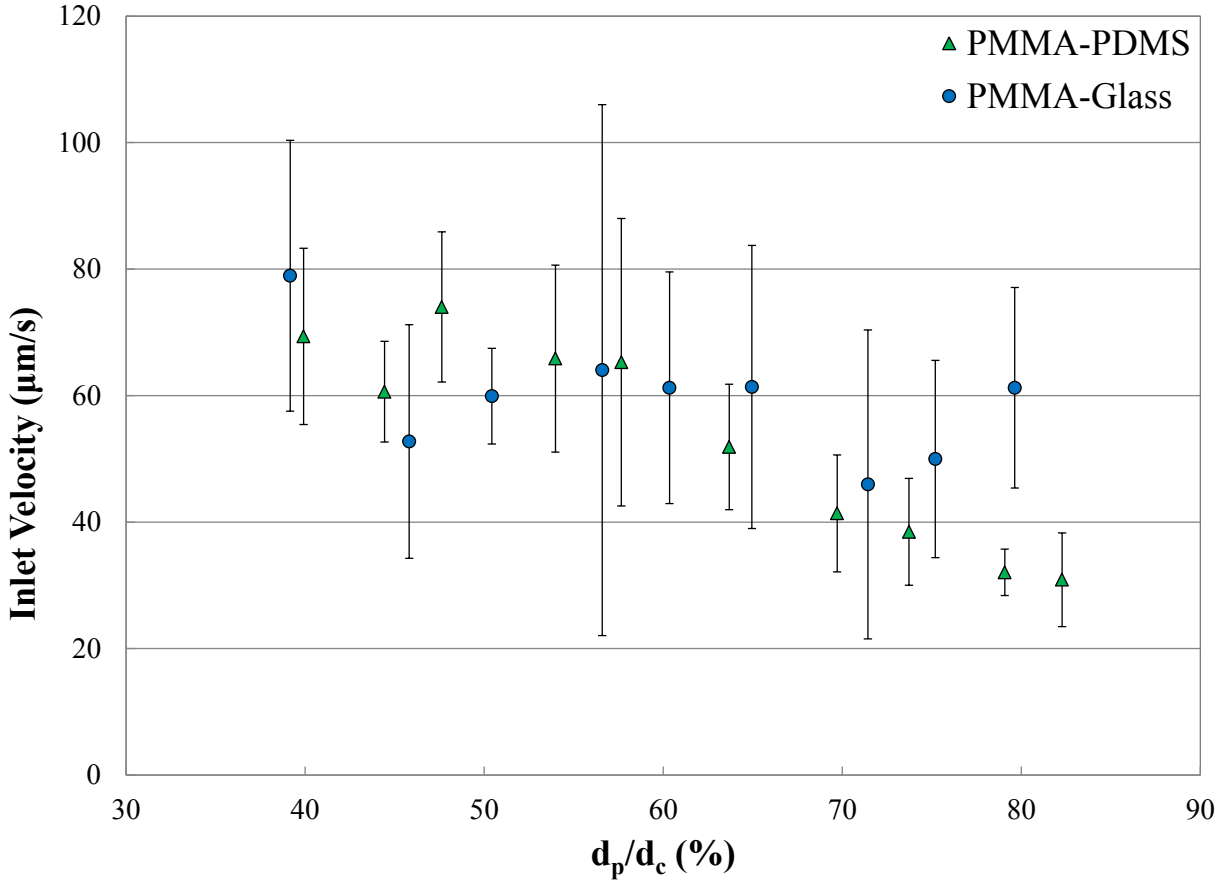

Figure 4.4: A comparison of the experimental results for microparticle detachment in a microchannel, where d_p is the diameter of the particle and d_c is the diameter of the channel. In the legend, the first material corresponds to the particle and the second material corresponds to the channel.

4.2.2 Forces Acting on Each Microparticle

Once the trials were completed, the forces due to gravity (F_G) and buoyancy (F_B) were calculated using **Equation 2.19** and **Equation 2.20** and the COMSOL model was used to determine the forces due to drag (F_D) and lift (F_L). After these were found, the adhesion force

was defined as a function of the work of adhesion (W_A) as in **Equation 2.24** and W_A was found as a fitting parameter of the moment balance defined in **Equation 2.18**. Following this, the rolling moment, as defined in **Equation 2.6**, was calculated for each data point to ensure that a moment balance was appropriate to use for the system. Most of the particles had rolling moments between one and two, but a few of the smallest particles had rolling moments as low as 0.6. However, very few particles had this issue and the assumption that all of the particles experienced rolling motion can be considered true for the system as a whole. This matches experimental observations and confirms that a moment balance is the best option for relating the forces acting on the particle to one another. Sample calculations for all of these steps can be found in **Appendix G** and detailed results of these calculations can be found in **Appendix H**.

For all of the material combinations, the forces acting on each particle were plotted versus the ratio of the particle diameter to the channel diameter to compare the magnitudes of the forces relative to each other. A few trends are consistent, regardless of the material pairing. For all data sets, the force due to lift remains stable at a value close to zero while the forces due to gravity, buoyancy, and adhesion increase with particle diameter. While drag appears to remain close to zero, closer inspection shows that it also increases with particle size. This will be discussed in more detail in the next section.

For the first combination of materials, a glass particle in a PDMS channel, the forces acting on each particle are shown in **Figure 4.5**. From the figure, it can be seen that the magnitude of the adhesion force is on the same scale as the forces due to gravity and buoyancy, which are significantly larger than the forces due to drag or lift.

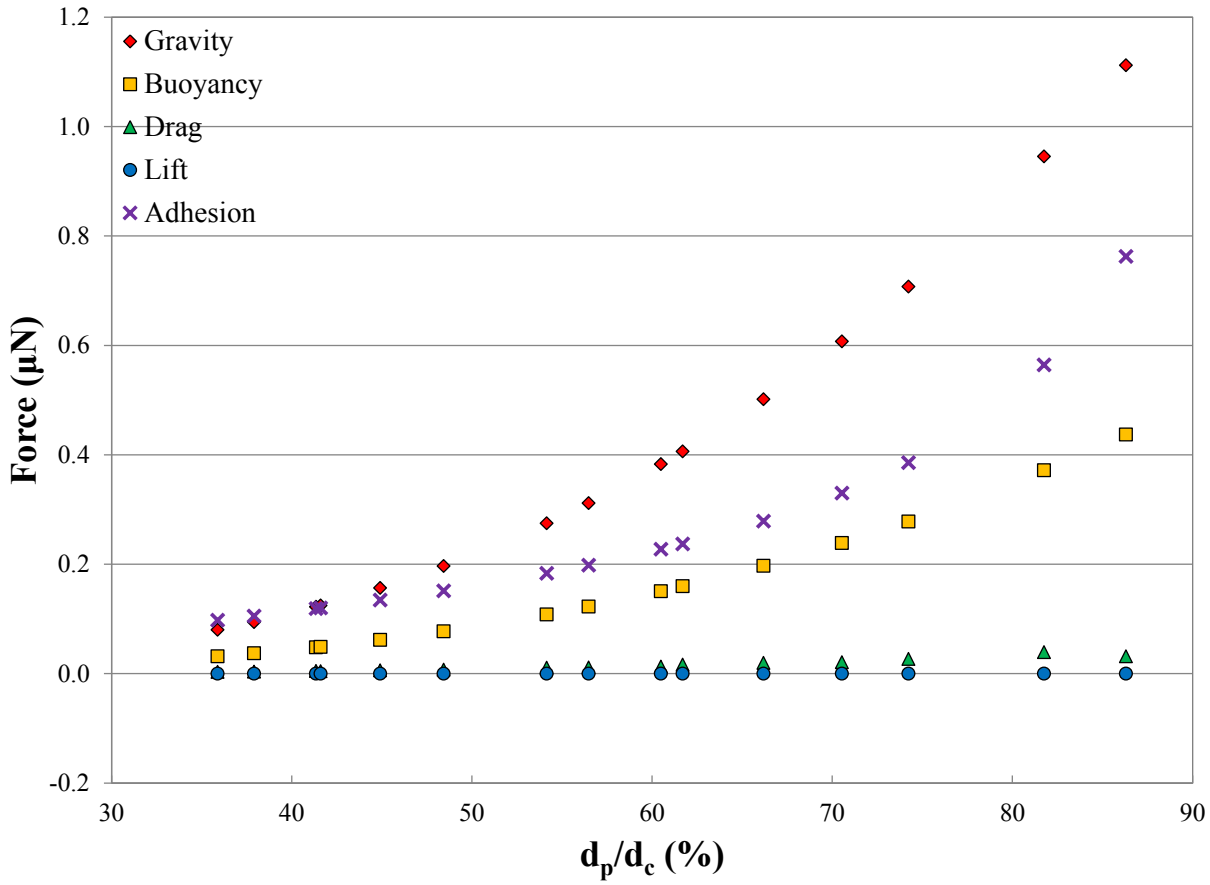

Figure 4.5: The forces acting on glass microparticles in a PDMS channel at the point of particle detachment, where d_p is the diameter of the glass particle and d_c is the diameter of the PDMS microchannel. For the PDMS microchannel, $d_c = 510\ \mu m$.

For the next combination of materials, a glass particle in a glass channel, the forces acting on each particle are shown in **Figure 4.6**. In this figure, it can be seen that the adhesion forces are by far the strongest forces acting on the glass particle. It is suspected that this behavior is due to the surface chemistry of glass and will be discussed further in Section 4.2.4.

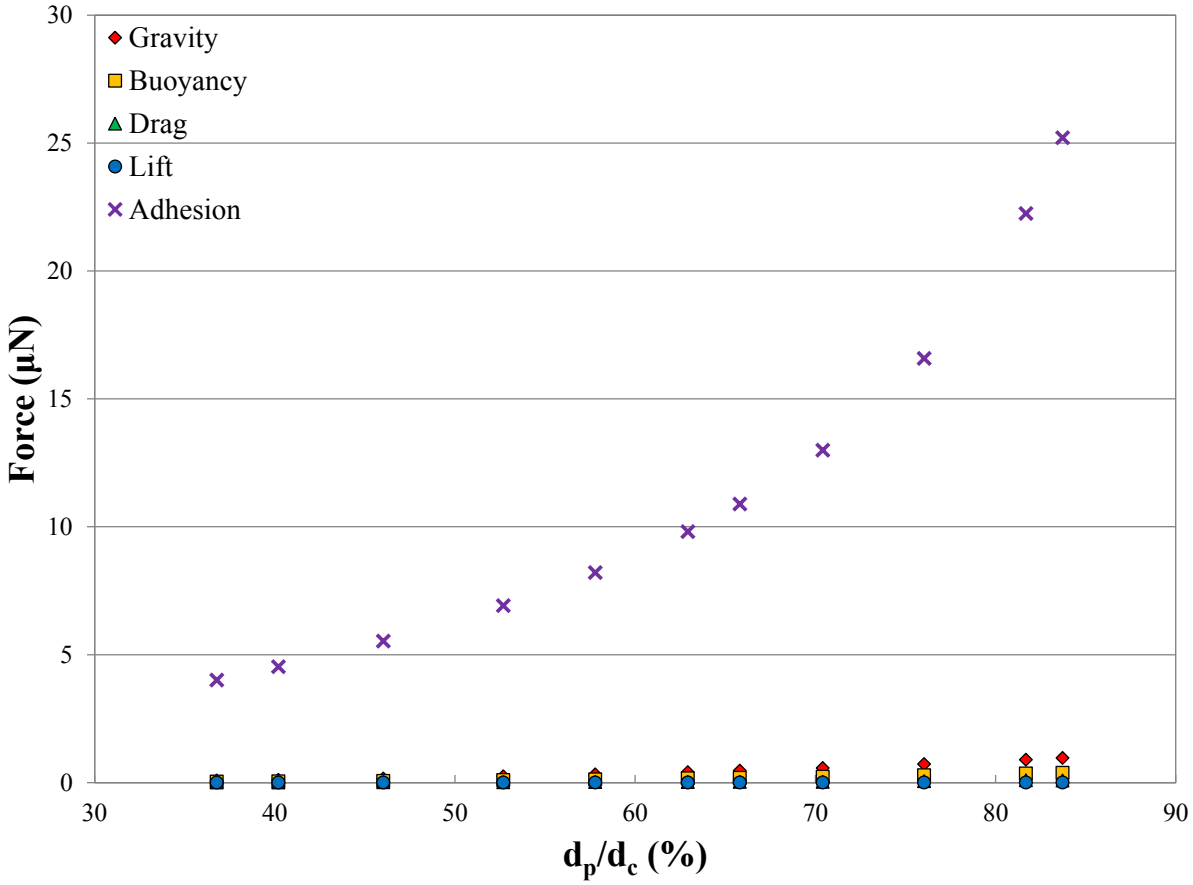

Figure 4.6: The forces acting on a glass microparticle in a glass channel at the point of detachment, where d_p is the diameter of the glass particle and d_c is the diameter of the glass microchannel. For the glass microchannel, $d_c = 500\ \mu m$.

For the next combination of materials, a PMMA particle in a PDMS channel, the forces acting on each particle are shown in **Figure 4.7**. In this figure, it can be seen that the adhesion forces are smaller than the forces due to gravity or buoyancy, but are still significantly larger than both the drag and lift forces acting on the particle.

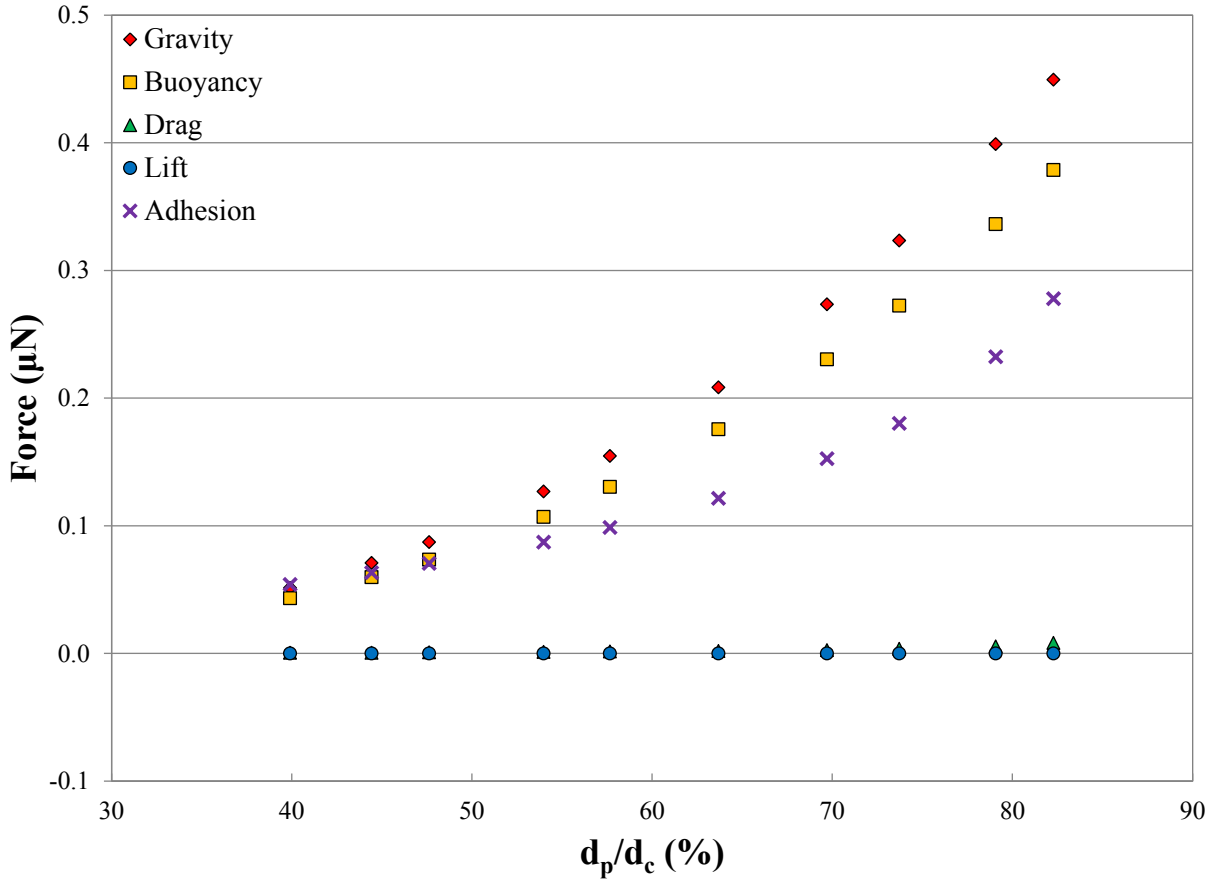

Figure 4.7: The forces acting on a PMMA microparticle in a PDMS channel at the point of detachment, where d_p is the diameter of the PMMA particle and d_c is the diameter of the PDMS microchannel. For the PDMS microchannel, $d_c = 510\ \mu m$.

For the last combination of materials, a PMMA particle in a glass channel, the forces acting on each particle are shown in **Figure 4.8**. In this figure, it can be seen that the adhesion forces are quite a bit larger than the forces due to gravity or buoyancy, but not to the extent of the glass particles in a glass channel.

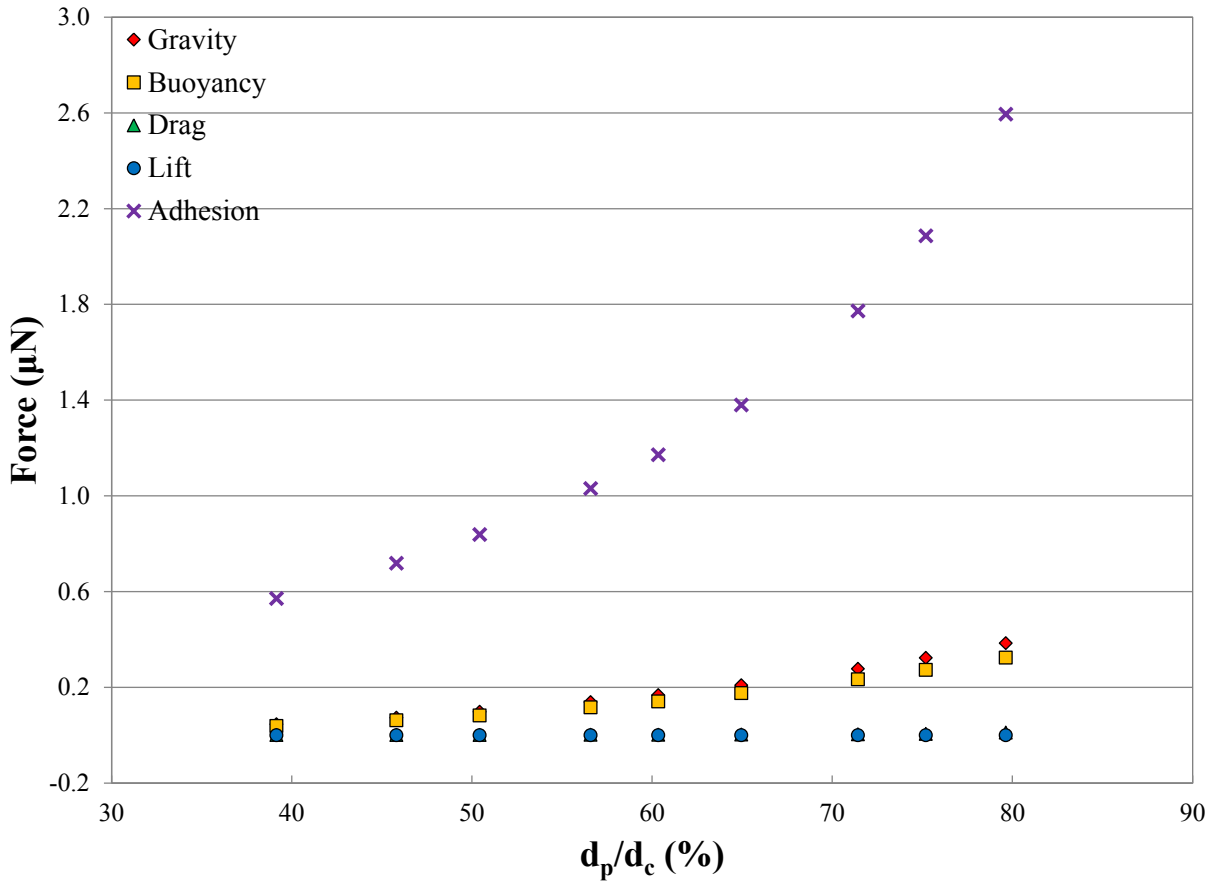

Figure 4.8: The forces acting on a PMMA microparticle in a glass channel at the point of detachment, where d_p is the diameter of the PMMA particle and d_c is the diameter of the glass microchannel. For the glass microchannel, $d_c = 500\ \mu m$.

4.2.3 Drag Force Analysis

In the overall moment balance for the system, drag plays a crucial role as the only force pushing the particle forward against the friction induced by the other forces. However, in the force comparisons above, drag appears to be almost zero relative to the other forces and no trends can be observed due to the necessary scaling on the plots. To get a closer look at the behavior of the drag force acting on the particles, the drag force from each material pairing is plotted in **Figure 4.9**, below.

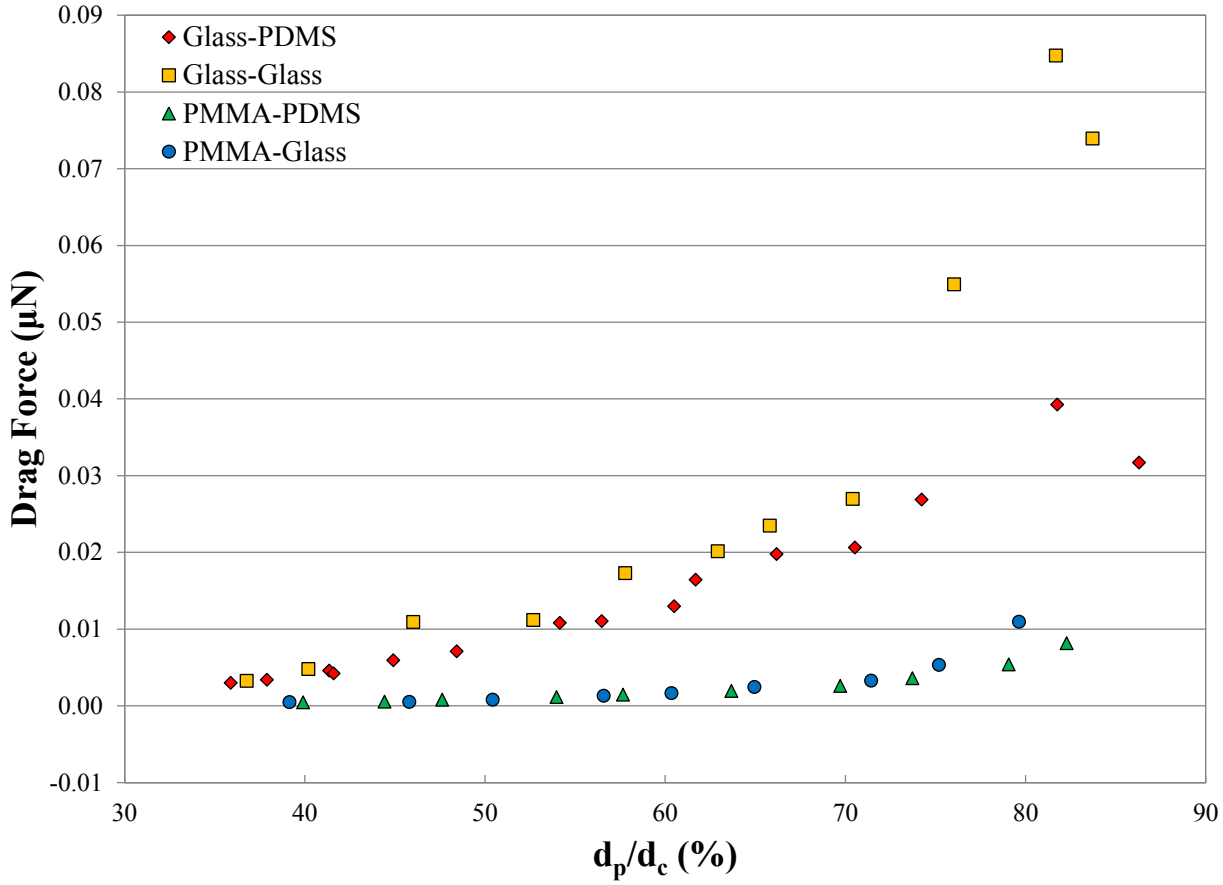

Figure 4.9: A comparison of the drag force acting on the particles at the point of detachment for each material pairing. where d_p is the diameter of the particle and d_c is the diameter of the microchannel. In the legend, the first material corresponds to the particle and the second material corresponds to the channel. For the glass microchannel, $d_c = 500\ \mu m$. For the PDMS microchannel, $d_c = 510\ \mu m$.

From this figure, it can be seen that the drag force acting on the glass particles is higher than the drag on the PMMA particles. This result can be attributed to the density of the materials. As discussed earlier, the glass particles are denser than the PMMA particles, indicating that gravity acts more strongly on a glass particle than a PMMA one of the same size. This means that the glass particles require a larger fluid velocity to induce detachment. As expressed in Stoke's Law, shown in **Equation 2.21**, drag is directly related to the velocity of the fluid, so denser particles require more drag to overcome the gravitational forces and detach from the channel wall.

One trend present in this graph that cannot be explained by Stoke's definition of drag is the relationship between drag force and particle diameter. According to Stoke's law, drag should be linear with respect to particle diameter. However, this is not how drag behaves in this system; instead, it increases exponentially with particle diameter. This behavior is due to the confined geometry of the system. As the particle size increases, it eventually starts to block the channel and impede fluid flow. As this occurs, the fluid is forced to increase its velocity to pass through the smaller opening. It also increases the pressure pushing the particle forward. These two components, viscous forces and pressure forces, work together to make up the total drag force acting on the particle. Traditional models for drag force, such as Stoke's law, cannot account for the velocity and pressure gradients created around the particle, making them impractical for this system. This is why a COMSOL model was required to determine the drag forces acting on the particles.

4.2.4 Adhesion Force Analysis

To take a closer look at the adhesion force, the work of adhesion can be examined. Returning to **Equation 2.24**, the adhesion force is directly related to the work of adhesion for any given material pairing, as shown below:

$$F_{A_{JKR}} = 1.5\pi W_A \left(\frac{d_{p,eff}}{2}\right) \tag{2.24}$$

The work of adhesion is constant for any given material pairing and is independent of the geometry of the system, making W_A an ideal parameter for comparing the adhesion forces between material pairings. The values of W_A were determined by fitting the experimental data to

the moment balance and can be found in **Table 4.1** below. While error could not be readily found for these values, a visual representation of the accuracy of W_A as a fitting parameter can be seen in **Figure H.1** to **Figure H.4** in **Appendix H**.

Table 4.1: The work of adhesion (W_A) calculated for the four different material pairings

Particle Material	Channel Material	W_A (μN/m)
Glass	PDMS	177
Glass	Glass	7,157
PMMA	PDMS	85
PMMA	Glass	936

Clearly, the glass particles in the glass channel experienced the most adhesion, with a work of adhesion almost ten times larger than any of the other material pairings. However, even the PMMA particles in the glass channel had a fairly large work of adhesion relative to the other values. Combining this parameter with the trends observed for the magnitude of the adhesion force relative to the other forces, it can be concluded that the material of the microchannel had a larger effect on the adhesive forces than the material of the particle.

While the definitive cause of this adhesive behavior is unknown, one potential reason is the surface chemistry of glass. Glass is primarily made up of silica (SiO_2), which ordinarily has a negative surface charge. On a glass surface submersed in water, the exposed oxygen and silicon atoms have a dangling bond, so each surface atom has more electrons than will fit in its valence shell. To compensate for this, the glass surface pulls hydrogen ions from the water to form silanol groups on its surface. A sketch of this behavior can be seen in **Figure 4.10**.

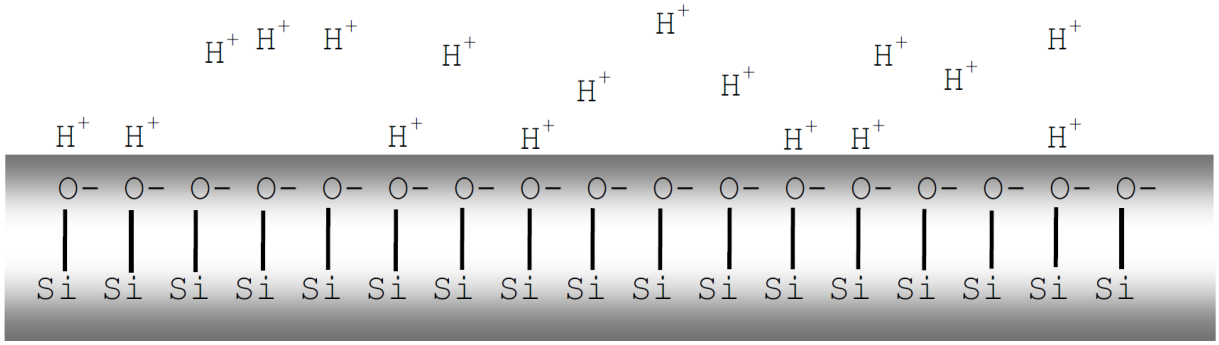

Figure 4.10: A visualization of a glass surface in contact with water. At the interface, glass forms silanol groups, causing the liquid coating the surface to become positively charged [1].

On the macro scale, this is almost imperceptible and does not have any significant effect. However, it is much more noticeable on the micro scale. In glass microfluidics, this phenomenon is actually used to induce electro-osmotic flow, which is when a fluid is propelled through a microchannel by a voltage. When the voltage is applied to the fluid, the positively charged hydrogen ions near the glass surface are pulled with the direction of the voltage. As these ions move, the rest of the fluid is dragged along, causing bulk plug flow [3]. While this flow mechanism is not being used in this application, the presence of so many hydrogen ions on the glass surface may play a part in the strong adhesion force of particles to the glass channel. Not only will the positive charge of the fluid near the surface attract the negatively charged surface of the glass particles, but the excess of hydrogen atoms may be responsible for some amount of hydrogen bonding between the two surfaces. Yet, this is currently just speculation. To prove that the adhesion is due in part to the presence of hydrogen ions, the experiments would have to be redone using a strongly alkali solution instead of the surfactant solution. In such a solution, there would not be enough hydrogen atoms available to fully coat the surface, which, if this theory is correct, should result in a decrease in adhesion. However, there would still be positive ions

present in the alkali solution, allowing surface charge to continue playing a role in the attractive forces. In order to analyze the effect of surface charge on adhesion, the glass channels would need to be treated with a passivating coating. These coatings act to neutralize the charge present on glass surfaces and are usually used to suppress electro-osmotic flow. In this case, a passivating coating would reduce the presence of the surface charge and prevent the accumulation of hydrogen ions.

As stated previously, glass is primarily made up of silica (SiO_2), but different variations of glass have different formulations and properties. In these experiments, the glass particles are made from soda-lime glass and the glass channels are made from borosilicate glass. Soda-lime glass generally contains 72% silica, 15% sodium oxide, 9% calcium oxide, with the remaining 4% miscellaneous minor ingredients. Borosilicate glass contains about 80% silica, 13% boric trioxide, 4% sodium oxide, and 2% alumina [16]. This means that, despite the different additives, both the glass particles and the glass channels have similar amounts of silica in them. However, this possible explanation for adhesion relies on the exposed surface area of a given material and the surface area on the inside of the glass channel is significantly larger than the surface area of a single microsphere. Therefore, it is reasonable to see a much larger adhesion for a polymer particle in a glass channel than for a glass particle in a polymer channel, which is the behavior demonstrated by the particles in this system.

5. CONCLUSIONS AND FUTURE WORK

The objectives of this study were 1) to develop a simple and inexpensive method to produce monodisperse polymer microparticles, 2) to examine the detachment behavior of microparticles in a microchannel, and 3) to characterize the adhesion forces acting between a microparticle and a microchannel for different material pairings.

While a technique to produce liquid-filled polymer capsules was not successfully developed, the first objective was completed for the production of solid polymer microparticles. A simple microfluidic device consisting of a glass capillary and a needle was constructed and used to successfully produce monodisperse polymer microparticles. This device was able to be used for different material combinations and the size of the particles produced could be fine-tuned to fit the specifications of the project. To determine if the device met the goal of being inexpensive, a brief breakdown of component prices was done. From Hamilton, the manufacturer of the needles, a package of six 30 gauge needles currently costs $54.00, which makes each needle worth $9.00 [17]. From Harvard Apparatus, the manufacturer of the capillaries, a package of 500 glass capillaries with the appropriate dimensions costs $56.00, making each capillary worth $0.11 [18]. Therefore, the total cost of each device is $9.11, which can confidently be described as inexpensive. While this device was ideal for producing the small quantities of particles necessary for this project, it does not have a high throughput and large scale production would be difficult, if not impossible, for a single device. However, scaling up production would be possible by operating many devices in parallel, which would easily be possible due to the

miniscule cost of each device. Overall, the microfluidic device developed over the course of this project exceeded expectations and the first objective of this study can be considered complete.

The second objective was also accomplished during this project through the examination of the velocity required to detach microparticles of varying sizes and materials from the wall of a microchannel. Through this study, it was determined that, at some particle to channel diameter ratio between 50 and 60%, particles of all materials require lower fluid velocities to detach from a microchannel wall. This ratio corresponds to the point where the drag forces exerted by the fluid increase as the particle occupies more of the cross-sectional area of the channel, overwhelming the gravitational and adhesive forces keeping the particle attached to the wall. This observation can be used as a general rule-of-thumb for determining how quickly a fluid needs to be flowing to keep solid particulates from settling out of the stream.

The last objective of this project was to characterize the adhesion force acting between a particle and a channel wall. In the past, the literature has assumed that the only adhesive forces acting on a particle were due to van der Waals interactions. However, this is definitely not applicable for this system; instead, the JRK theory for elastic contact was found to be much more appropriate. This theory allows the adhesive force to be expressed in terms of the work of adhesion and the effective diameter of the particle. Using the moment balance on the particle, the work of adhesion was able to be calculated for each material pairing, which served as a convenient parameter for comparison. It was found that glass channels exhibit significantly more adhesive properties than PDMS channels. To a lesser extent, this trend was also true for glass particles. It is suspected that the surface chemistry of glass is responsible for this adhesion, but

this theory is currently just speculation. Whatever the cause, the identity of each material had a significant effect on the adhesive force between the particle and the channel, more than could be explained only through van der Waals forces.

In the future, work should be done to study the practicality of scaling up the production of polymer microspheres using the device developed for this study. Other research could be done to investigate the possible types of polymers that can be produced in the device and what flow rates should be used to make differently sized particles. For the microparticle detachment studies, more experiments should be run to look at the adhesive forces acting between different material pairings and confirm that the JRK model for adhesion is the best option. Other studies should be done to examine the cause of the strong adhesive forces exhibited by the glass. As mentioned previously, the theory presented in this report is not confirmed, but could be through further experimentation using a strongly basic solution or a passivating coating.

LIST OF REFERENCES

[1] Adams, Thomas M., and Richard A. Layton. *Introductory MEMS: Fabrication and Applications*. New York: Springer, 2010.

[2] Nguyen, Nam-Trung, and Steven T. Wereley. *Fundamentals and Applications of Microfluidics*. Boston: Artech House, 2006. *Ebrary*. ProQuest. <http://site.ebrary.com/lib/rosehulman/reader.action?docID=10359090>.

[3] Senturia, Stephen D. "Microsystems for DNA Amplification." *Microsystem Design*. Boston: Kluwer Academic, 2001. 605-27.

[4] Glasgow, I. K., H. C. Zeringue, D. J. Beebe, Seong-Jun Choi, J. T. Lyman, N. G. Chan, and M. B. Wheeler. "Handling Individual Mammalian Embryos Using Microfluidics." *IEEE Transactions on Biomedical Engineering* 48.5 (2001): 570-78. *IEEE Xplore*. IEEE, May 2001. <http://ieeexplore.ieee.org/xpl/articleDetails.jsp?arnumber=918596>.

[5] Bader, Rebecca A., and David A. Putnam. *Engineering Polymer Systems for Improved Drug Delivery*. Hoboken, New Jersey: Wiley, 2013. *EBSCOhost*. <http://web.a.ebscohost.com/ehost/detail/detail?sid=80fcb0b2-badb-47ab-aea8-7a23d9b8b8db%40sessionmgr4002&vid=0&hid=4214&bdata=JnNpdGU9ZWhvc3QtbGl2ZSZzY29wZT1zaXRl#db=nlebk&AN=688375>.

[6] Erb, Randall M., Dominik Obrist, Philipp W. Chen, Julia Studer, and André R. Studart. "Predicting Sizes of Droplets Made by Microfluidic Flow-induced Dripping." *Soft Matter* 7.19 (2011): 8757.

[7] Shukla, Nimisha, and Kimberly H. Henthorn. "Effect of Relative Particle Size on Large Particle Detachment from a Microchannel." *Microfluidics and Nanofluidics Microfluid Nanofluid* 6.4 (2008): 521-27.

[8] Salama, Abd-Elhady Mohamed Aly Mohamed. "Gas-Side Particulate Fouling in Biomass Gasifiers." Thesis. Proefschrift Technische Universiteit Eindhoven, 2005.

[9] Essawey, Abdelmaged Hafez Ibrahim. "Microparticle Detachment from Surfaces by Fluid Flow." Diss. 2004.

[10] Hiemenz, Paul C., and Raj Rajagopalan. *Principles of Colloid and Surface Chemistry*. 3rd ed. New York: Marcel Dekker, 1997.

[11] O'Neill, M.E. "A Sphere in Contact with a Plane Wall in a Slow Linear Shear Flow." *Chemical Engineering Science* 23.11 (1968): 1293-298.

[12] Leighton, David, and Andreas Acrivos. "The Lift on a Small Sphere Touching a Plane in the Presence of a Simple Shear Flow." *Journal of Applied Mathematics and Physics* 36.1 (1985): 174-78.

[13] Cabrejos, Francisco J. "Incipient Motion of Solid Particles in Pneumatic Conveying." Thesis. University of Pittsburgh, 1991.

[14] Nurumbetov, Gabit, Nicholas Ballard, and Stefan A. F. Bon. "A Simple Microfluidic Device for Fabrication of Double Emulsion Droplets and Polymer Microcapsules." *Polymer Chemistry* 3.4 (2012): 1043.

[15] "Price List: Precision Grade Glass Spheres (Class V)." Price Sheets. Mosci Corporation, n.d. <http://www.mo-sci.com/price-sheets/>.

[16] Seymour, Raymond B., and Charles E. Carraher. *Polymer Chemistry: An Introduction*. 4th ed. New York: Marcel Dekker, 1996.

[17] "30 Gauge, Metal Hub NDL, Custom Length (0.375 to 12 In), Point Style 2, 3, or 4, 6/PK." *Hamilton*. Hamilton Company, n.d. <http://www.hamiltoncompany.com/products/syringes-and-needles/needles/luer-lock-needles/metal-hub-needles/30-gauge-Metal-Hub-NDL-custom-length-0375-to-12-in-point-style-2-3-or-4-6PK>.

[18] "Clark Borosilicate Standard Wall." *Harvard Apparatus*. Harvard Apparatus, n.d. <http://www.harvardapparatus.com/clark-borosilicate-standard-wall.html>.

[19] Hunter, Robert J. *Introduction to Modern Colloid Science*. Oxford: Oxford UP, 1993.

APPENDICES

APPENDIX A

Details of the COMSOL Model

To find the drag and lift forces acting on the particles in the microchannel, a computational fluid dynamics simulation was made to model the flow of water through a small channel with a spherical obstruction fixed to the bottom. This simulation was created using the COMSOL Multiphysics® 5.1 software, produced by COMSOL Incorporated.

This model is a three dimensional simulation that uses the laminar flow physics package to compute the velocity and pressure fields for the flow of a single-phase fluid in the laminar flow regime using the Navier-Stokes equations for conservation of momentum and the continuity equation for conservation of mass . All of the measurements taken experimentally were done at very low flow rates in micro-scale channels, so it is safe to assume that fluid flow around the particles was laminar. This model was designed to compute the forces acting on the particle at the point of detachment, so a stationary study was used rather than a time dependent study.

First, a set of parameters was defined so that future changes could be made easily. The parameters that were customized to match experimental conditions were the channel inner diameter (d_c), the particle diameter (d_p), and the volumetric flowrate required for particle detachment (Q). The other parameters were set as constants and included the channel length, which was set as $77\ mm$, and the distance between the particle and the entrance of the channel, which was set as $25\ mm$. These dimensions ensured that the channel was long enough for laminar flow to develop fully before reaching the particle.

For the geometry of the system, all coordinates are expressed as (x, y, z). To model the microchannel, a cylinder with a diameter of d_c and the length specified above was constructed at the coordinates (0, 0, 0) along the x-axis with no rotation. A sphere was then built with a radius of d_p at the coordinates ($25\ mm, -d_c/2 + d_p/2, 0$). This oriented the sphere so that it was $25\ mm$ away from the entrance of the cylinder and sitting on the bottom of the cylinder. A difference was then taken to remove the sphere from the cylinder, leaving behind the channel missing a spherical portion. An image of this assembly can be found in **Figure A.1**. Once the geometry was built, water was selected as the material and applied to the entire component. Overall, this structure represents the water in the microchannel flowing around the particle-sized sphere that was removed. Because the drag and lift forces are only dependent on the geometry of the system, not the material properties of the particle or the channel, this model is sufficient to calculate the forces.

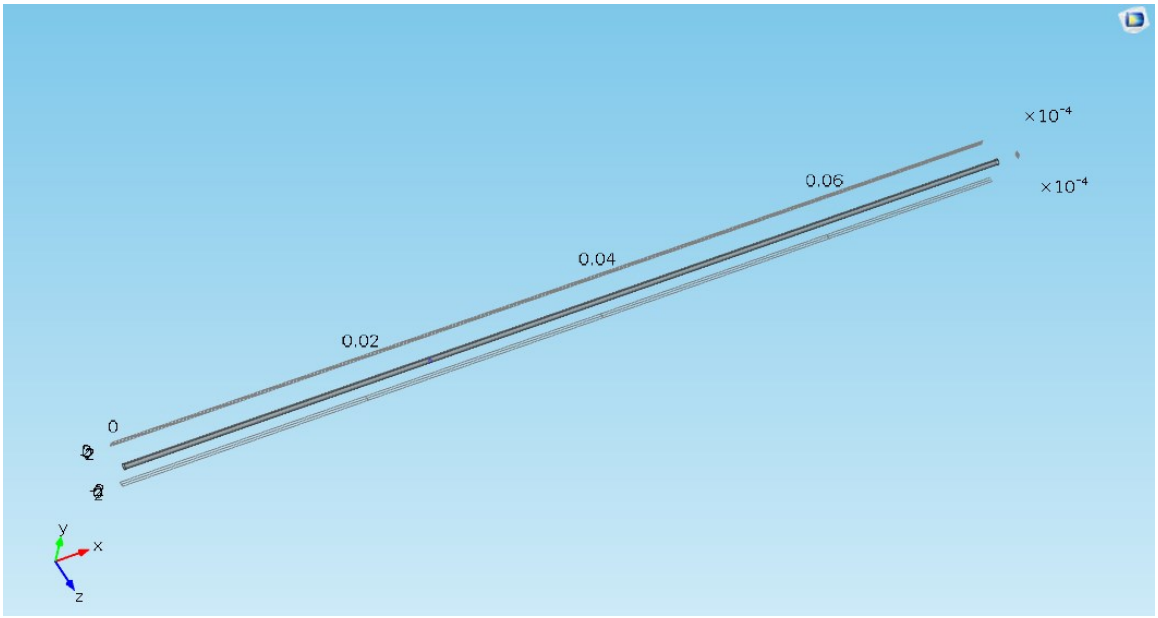

Figure A.1: The geometry of the COMSOL simulation, consisting of a tube with a spherical section removed, which can be seen slightly past the 0.02 marker on the x-axis.

Once the structure was finished, the laminar physics were applied to the system. First, the fluid properties were applied to the water, using the density and dynamic viscosity from the material library and setting the temperature to 20˚C, the room temperature of the laboratory where experiments were completed. Next, the initial values of the system were set so that the velocity field was zero in all directions and so that the pressure was also zero. These settings ensured that the fluid was fully still before any flow was simulated. The next step was to set the boundary conditions of the system. The walls of every surface except the two ends of the cylinder were set to no slip boundary conditions while the inlet of the cylinder was set to have a normal inflow velocity of $Q/(\pi d_c^2/4)$, which converts the volumetric flow rate to the equivalent velocity of the fluid traveling through the channel. The other end of the cylinder was set as the outlet with the boundary condition of zero pressure, modeling that the other end of the channel was open to the atmosphere.

Following the application of the physics, a physics-controlled mesh with a normal element size was built and the simulation was run. A sample velocity profile from the completed simulation can be seen in **Figure A.2**. After the simulation was complete, the drag and lift forces were calculated as surface integrations. These surface integrations were done only over the walls of the sphere in the channel and the expressions “spf.T_stressx” and “spf.T_stressy” were used to calculate the total stress in the x and y directions, respectively. According to the geometry of the system, the stress in the x direction corresponds to the drag force and the stress in the y direction corresponds to the lift force. However, these stresses are acting on the fluid, not on the sphere, so the negative of these stresses was taken as the drag and lift forces acting on the particle. The full results from these simulations can be found in **Appendix H**.

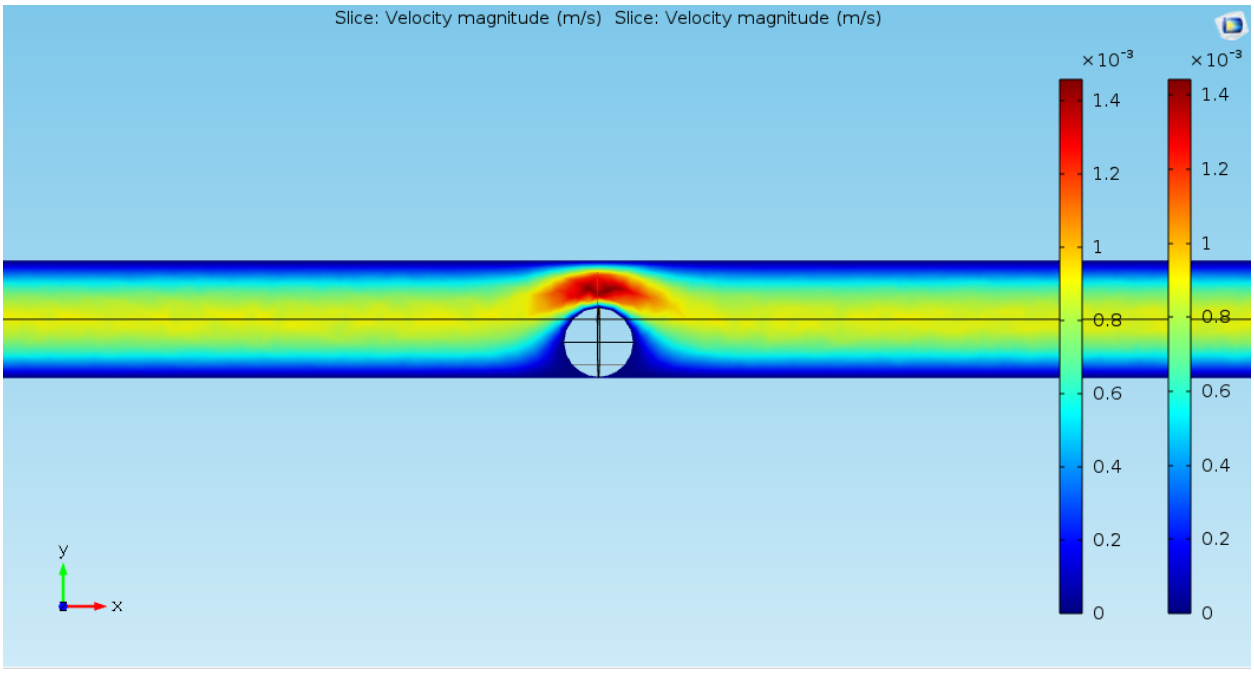

Figure A.2: The velocity profile of the fluid with a flow rate of $Q = 5.71\ \mu L/min$ flowing around a particle with a diameter of $308.53 \mu m$ in a channel with a diameter of $510\ \mu m$. This corresponds to experimental results for a glass particle of the same size in the PDMS microchannel. From this simulation, $F_D = 1.2963 \times 10^{-8} N$ and $F_L = 4.1218 \times 10^{-11} N$.

Aside from using COMSOL to calculate the lift and drag forces, the materials library was also used as the literature source for the Young's modulus and Poisson ratio for most of the materials. For the glass properties, the entry for borosilicate glass in the MEMS-Insulators material library was used for both properties. For PDMS, the entry for polydimethylsiloxane was used for the Poisson ratio. For PMMA, the entry for poly methyl methacrylate was used for both properties. All of these values can be found in **Appendix H**.

APPENDIX B

Materials and Equipment Details

Table B.1: Materials and equipment for the double-emulsion droplet device

Components of the Microfluidic Device

Description	Material	Dimensions (mm)	Manufacturer	Part Number
Capillary	Borosilicate Glass	3.0 OD x 1.62 ID	Harvard Apparatus	30-0080
Capillary	Borosilicate Glass	1.0 OD x 0.50 ID	Harvard Apparatus	30-0018
Needle	304 Stainless Steel	0.31 OD x 0.16 ID	Hamilton	7748-16
Tubing	C-Flex elastomer	2.4 OD x 0.8 ID	Cole-Parmer	06422-01
Syringe, 1.0mL	Glass, PTFE Luer	4.61 ID	Hamilton	81320
Syringe, 500µL	Glass, PTFE Luer	3.26 ID	Hamilton	81220
Syringe, 100µL	Glass, PTFE Luer	1.46 ID	Hamilton	81020
Luer Adapter	Polypropylene	1.6 ID	Cole-Parmer	45508-00

Equipment Used to Operate the Microfluidic Device

Description	Manufacturer	Model	Serial Number
Syringe Pump - 1	Aladdin	AL-4000	283746
Syringe Pump - 6	Aladdin	ALADDIN-6000	254181
UV Light System	Electro-Life Corporation	ELC-500-110	7600039
Inverted Microscope	Olympus Corporation	CKX41SF	0L36073
Microscope Camera	Olympus Corporation	SC30	0J46504

Table B.2: Materials and equipment for the single-emulsion droplet device

Components of the Microfluidic Device

Description	Material	Dimensions (mm)	Manufacturer	Part Number
Capillary	Borosilicate Glass	1.0 OD x 0.50 ID	Harvard Apparatus	30-0018
Needle	304 Stainless Steel	0.31 OD x 0.16 ID	Hamilton	7748-16
Tubing	C-Flex elastomer	2.4 OD x 0.8 ID	Cole-Parmer	06422-01
Syringe, 1.0mL	Glass, PTFE Luer	4.61 ID	Hamilton	81320
Syringe, 100µL	Glass, PTFE Luer	1.46 ID	Hamilton	81020
Luer Adapter	Polypropylene	1.6 ID	Cole-Parmer	45508-00

Equipment Used to Operate the Microfluidic Device

Description	Manufacturer	Model	Serial Number
Syringe Pump - 1	Aladdin	AL-4000	283746
Syringe Pump - 6	Aladdin	ALADDIN-6000	254181
UV Light System	Electro-Life Corporation	ELC-500-110	7600039
Inverted Microscope	Olympus Corporation	CKX41SF	0L36073
Microscope Camera	Olympus Corporation	SC30	0J46504

Table B.3: Chemicals used to synthesize the microparticles

CAS Number	Abbreviation	Sigma Aldrich Product Number	IUPAC Name
80-62-6	MMA	M55909	Methyl methacrylate
97-90-5	EGDMA	335681	Ethylene glycol dimethacrylate
106-91-2	GMA	151238	Glycidyl methacrylate
5888-33-5	IBA	392103	Isobornyl acrylate
9002-89-5	PVA	363081	Poly(vinyl alcohol)
9004-67-5	MC	274429	Methyl cellulose
24650-42-8	DMPA	196118	2,2-Dimethoxy-2-phenylacetophenone
71868-10-5	MTMP	405639	2-Methyl-4′-(methylthio)-2-morpholinopropiophenone

Table B.4: Materials used to make the PDMS microchannels

Description	Manufacturer	Part Number
Sylgard® 184 Silicone Elastomer Kit	Dow Corning Corporation	3097358-1004
PDMS Mold	Custom Built (see below)	N/A
25 Gauge Needle, 4”, pt 3	Hamilton	7748-11
Dry Film Release Agent	Sprayon	MR311

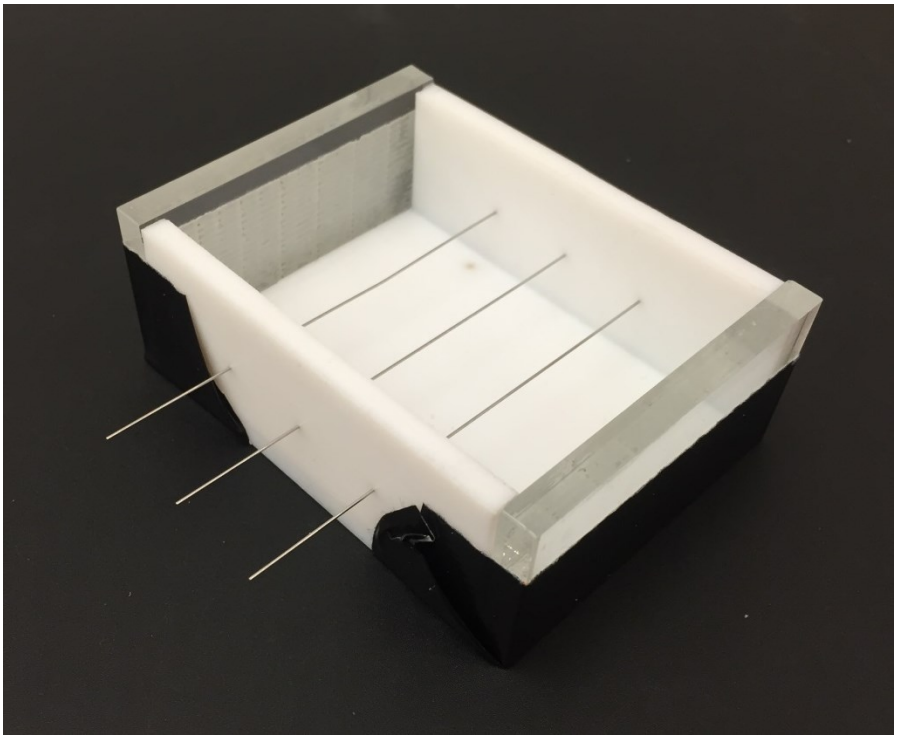

Figure B.1: The mold used to make the PDMS microchannels. This mold is a topless rectangular box 7.5 cm long, 5.5 cm wide, and 2.5 cm tall. The two shorter edges are separate pieces that are taped onto the center piece. In each of the two longer sides, three aligned holes are drilled through the wall of the mold, allowing three needles to be suspended in parallel approximately 1 cm above the bottom.

Table B.5: Materials and equipment for detachment experiments

Description	Manufacturer	Part Number
Syringe, 100µL	Hamilton	81020
Syringe, 5.0mL	Hamilton	81520
25 Gauge Needle, 1”	Hamilton	7750-16
30 Gauge Needle, 4”	Hamilton	7748-16
C-Flex Tubing	Cole-Parmer	06422-01
0.50mm ID Capillary	Harvard Apparatus	30-0018
Luer Adapter	Cole-Parmer	45508-00
TWEEN® 80, CAS 9005-65-6	Sigma Aldrich	P1754
PDMS Microchannel	Custom Made	N/A
Glass Microchannel Capillary, 0.5mm ID	Harvard Apparatus	30-0018
PMMA Microparticles	Custom Made	N/A
Class V Soda Lime Glass Spheres (-70+80 mesh)	MO-SCI	GL0191B5/180-212
Class IV Soda Lime Glass Spheres (-50+70 mesh)	MO-SCI	GL0191B4/212-300
Class IV Soda Lime Glass Spheres (-40+50 mesh)	MO-SCI	GL0191B4/300-425
Syringe Pump - 1	Aladdin	AL-4000 283746
Syringe Pump - 6	Aladdin	ALADDIN-6000 254181
Inverted Microscope	Olympus Corporation	CKX41SF-0L36073
Microscope Camera	Olympus Corporation	SC30-0J46504

APPENDIX C

Non-Stick Spray Side Investigation

During the process of making the PDMS microchannels, as described in Section 3.2.1, it was initially recommended that a non-stick spray be applied to the assembled mold before filling it with the un-cured PDMS. This non-stick spray was the dry film release agent Sprayon MR311, more details on this product can be found in **Appendix B**. While the non-stick spray made removing the PDMS microchannels from the mold easier and less susceptible to damage, the microchannels made using this technique were found to have very rough surfaces that caused significant disturbances in particle rolling behavior. From visual inspection during the spraying process, it was noticed that the non-stick spray created an uneven coating on the needles, making the spray the primary suspect for the surface roughness. To confirm this theory, a set of half-channels was made to compare the inner surface of the microchannels made with and without the non-stick spray. These half-channels were made using the same technique as described previously, with a couple modifications. First, the non-stick spray was applied to the entire mold with the exception of one of the needles, making a channel with the non-stick spray and one without. The other difference was that, instead of filling the mold completely with the uncured PDMS, it was only filled to cover half of the needle. This allowed for the close inspection of the inner surface of each half-channel to observe the effect that the non-stick spray had on the surface roughness of the microchannels. These half-channels can be seen in **Figure C.1**. Once the half-channels were cured completely and removed from the mold, they were inspected under the microscope. The microscope pictures for each half-channel can be seen in **Figure C.2**.

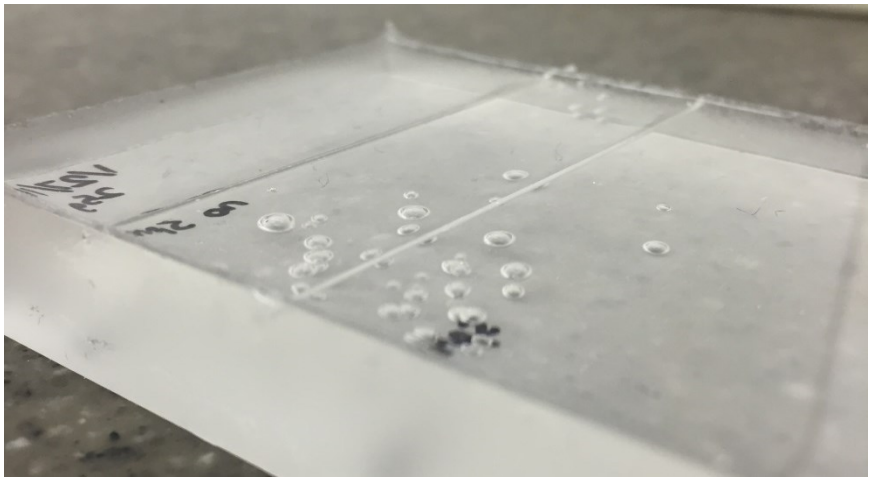

Figure C.1: The half-channels that were used to compare the effect of non-stick spray on the surface roughness of the microchannels. The channel on the right had the non-stick spray applied while the channel on the left did not.

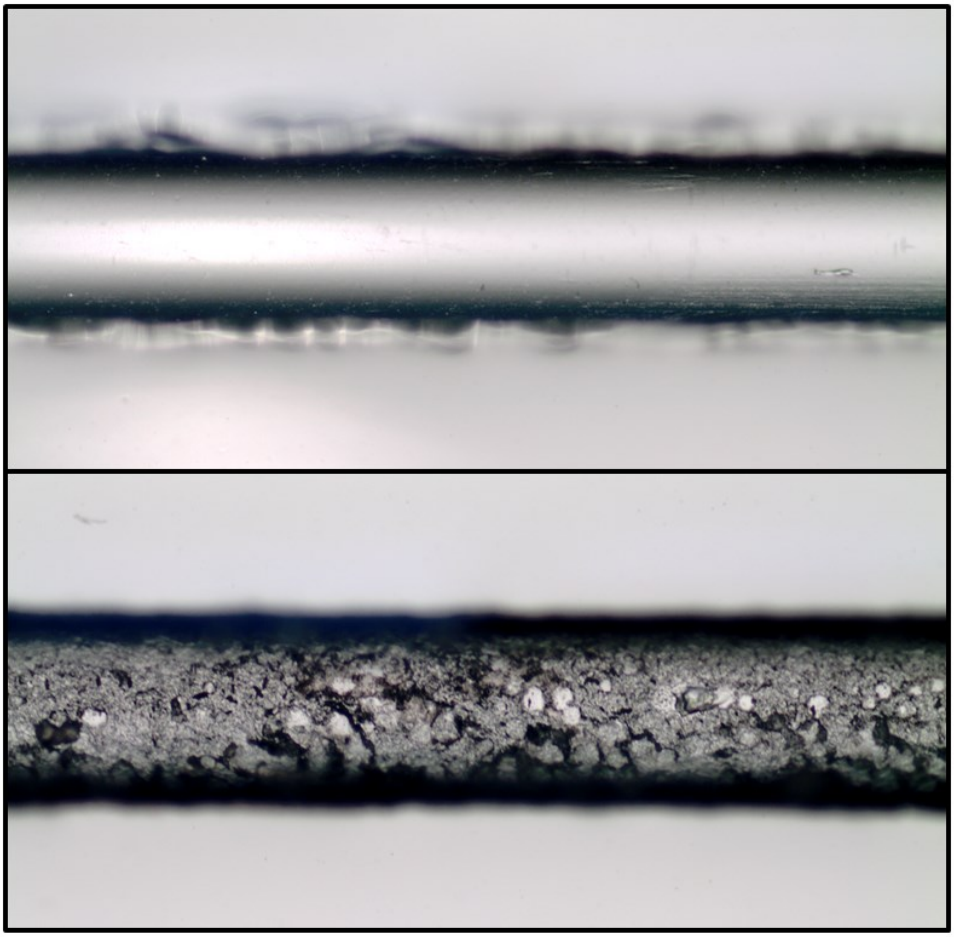

Figure C.2: The microscope images of the inner surfaces of the two half-channels. The top image is from the half-channel made without the non-stick spray and the bottom image is from the half-channel made with the non-stick spray.

From this comparison of the two half-channels, it is apparent that the use of the non-stick spray in the creation of the PDMS microchannels had a significant effect on the roughness of the inner surface of the microchannels. The spray produced extreme surface roughness, causing any microparticles in the channels to detach inconsistently and skewing detachment velocities. As a result of this side investigation, all PDMS microchannels used in the particle detachment testing were made without the use of the non-stick spray to ensure smooth surfaces and consistent results.

APPENDIX D

Settling Time Determination

During the microparticle detachment experiments described in Section 3.2.2, the microparticles were allowed to settle to the bottom of the microchannels before any attempts were made to dislodge them. To determine the amount of time required to ensure that the particles were definitely in contact with the bottom of the channel, the settling velocity of the particles was calculated, as shown in **Equation D.1**:

$$u_s = \frac{2(\rho_p - \rho_f)g}{9\mu}\left(\frac{d_p}{2}\right)^2 \tag{D.1}$$

where $u_s$is the settling velocity, ρ_p is the density of the particle, ρ_f is the density of the fluid, g is the acceleration due to gravity, μ is the dynamic viscosity of the fluid, and d_p is the diameter of the particle [19]. As seen in the equation above, as the size of the particle increases and the density of the particle decreases, u_s increases. In order to calculate the slowest possible settling velocity for the worst case scenario, the sample calculations below are done for a small particle size for the least dense particle material, PMMA. A sample calculation of the settling velocity for a PMMA particle with a diameter of $200\mu m$ is shown below.

$$u_s = \frac{2\left(1{,}184.4\ \frac{kg}{m^3} - 998.23\ \frac{kg}{m^3}\right)\left(9.81\frac{m}{s^2}\right)}{9\left(1.002\frac{kg}{s\cdot m}\right)}\left(\frac{200\times10^{-6}m}{2}\right)^2 = 4.05\times10^{-6}\frac{m}{s}$$

For a glass particle of the same size, the settling velocity is $3.35\times10^{-5}\,m/s$.

In a microchannel, the furthest distance the particle could fall would be if the top of the particle was touching the top of the channel. For the PDMS microchannel with a diameter of $510\ \mu m$ and a microparticle with a diameter of $200\ \mu m$, the largest settling distance would be $310\ \mu m$. If that particle was made of PMMA, the time required to allow the particle to settle would be $76.5\ s$, or approximately one minute and twenty seconds. As a precaution, this time was doubled and rounded up to the nearest minute, so the settling time allotted for each PMMA particle during experimentation was three minutes. For a glass microparticle of the same size and in the same channel, the time required to allow the particle to settle was $9.3\ s$. Again, the time allocated for settling during experimentation was doubled and rounded up, this time to one minute.

APPENDIX E

Experimental Results - Polymer Microparticle Production

Table E.1: Full results for the generation of poly(isobornyl acrylate) microparticles, where Q_1 is the volumetric flow rate of the inner phase IBA solution, Q_2 is the volumetric flow rate of the outer phase PVA solution, d_p is the average diameter of the particles in the sample, and n is the number of particles in the sample.

Q_1 (mL/min)	Q_2 (mL/min)	d_p (μm)	n
0.050	0.100	547.42 ± 2.00	10
0.050	0.150	505.22 ± 4.92	10
0.050	0.200	471.01 ± 3.43	10
0.025	0.150	453.24 ± 3.33	10
0.025	0.200	424.56 ± 3.49	10
0.025	0.250	410.15 ± 4.67	10
0.025	0.500	327.16 ± 14.69	32
0.025	0.550	318.79 ± 5.33	40
0.010	0.550	285.05 ± 8.38	33
0.005	0.550	268.09 ± 5.75	37
0.005	0.600	254.68 ± 5.52	41
0.005	0.700	236.92 ± 7.38	52
0.005	0.800	217.92 ± 3.13	63
0.005	0.900	210.76 ± 8.46	55
0.005	1.000	193.82 ± 4.19	49
0.005	1.100	180.17 ± 9.70	57
0.005	1.200	175.00 ± 5.78	70
0.005	1.300	180.52 ± 7.73	115
0.005	1.400	166.44 ± 4.93	85
0.005	1.500	155.67 ± 12.39	110
0.005	1.600	145.70 ± 4.10	129

Table E.2: Full results for the generation of poly(methyl methacrylate) microparticles, where Q_1 is the volumetric flow rate of the inner phase MMA solution, Q_2 is the volumetric flow rate of the outer phase MC solution, d_p is the average diameter of the particles in the sample, and n is the number of particles in the sample.

Q_1 (mL/min)	Q_2 (mL/min)	d_p (μm)	n
0.010	0.100	235.59 ± 15.35	20
0.010	0.200	219.13 ± 14.00	54
0.010	0.050	319.76 ± 30.59	20
0.010	0.025	367.89 ± 15.39	24
0.010	0.075	279.38 ± 30.72	42
0.010	0.150	230.91 ± 14.48	59
0.010	0.125	248.03 ± 32.20	43
0.010	0.175	200.96 ± 24.77	68
0.010	0.225	197.44 ± 16.01	84
0.010	0.250	199.86 ± 15.61	51
0.010	0.015	403.19 ± 31.24	26

APPENDIX F

Experimental Results - Microparticle Detachment

Table F.1: Full experimental results for the detachment of glass microparticles in a PDMS microchannel, where d_p is the diameter of the glass particle, d_c is the diameter of the PDMS microchannel, and Q is the volumetric flow rate required for the particle to detach from the bottom of the microchannel. The error on the average value of Q is the standard deviation of the data set. For the PDMS microchannel, $d_c = 510\ \mu m$.

d_p (μm)	d_p/d_c (%)	Detachment Flow Rate, Q (μL/min)							Average Q (μL/min)
183.03	35.89	10.00	7.00	6.00	5.50	10.00	7.00	9.00	7.79 ± 1.87
193.32	37.91	6.00	9.00	8.00	7.00	6.50	9.50	7.00	7.57 ± 1.30
210.91	41.35	9.00	7.00	8.00	9.50	8.00	7.00	-	8.08 ± 1.02
212.21	41.61	9.00	8.00	7.00	6.00	8.00	6.00	7.00	7.29 ± 1.11
229.05	44.91	8.00	10.00	6.50	6.00	11.50	8.50	6.00	8.07 ± 2.11
247.00	48.43	9.00	9.50	7.00	7.00	8.00	6.50	6.00	7.57 ± 1.30
276.18	54.15	5.00	7.50	5.00	6.00	9.00	10.50	10.50	7.64 ± 2.41
288.08	56.49	8.00	7.00	5.00	10.00	5.00	5.50	5.50	6.57 ± 1.88
308.53	60.50	6.00	6.00	5.00	5.50	5.00	5.50	7.00	5.71 ± 0.70
314.64	61.69	7.00	6.50	5.50	8.00	7.50	5.00	5.50	6.43 ± 1.13
337.58	66.19	5.00	4.50	5.50	5.50	7.00	6.00	4.50	5.43 ± 0.89
359.75	70.54	4.00	3.00	4.00	3.25	4.25	3.25	4.75	3.79 ± 0.64
378.58	74.23	4.50	3.00	2.50	3.50	3.50	3.00	3.50	3.36 ± 0.63
416.99	81.76	1.50	2.50	1.25	1.75	2.00	2.75	2.00	1.96 ± 0.53
440.15	86.30	0.80	0.60	0.80	0.60	1.20	0.50	0.80	0.76 ± 0.23

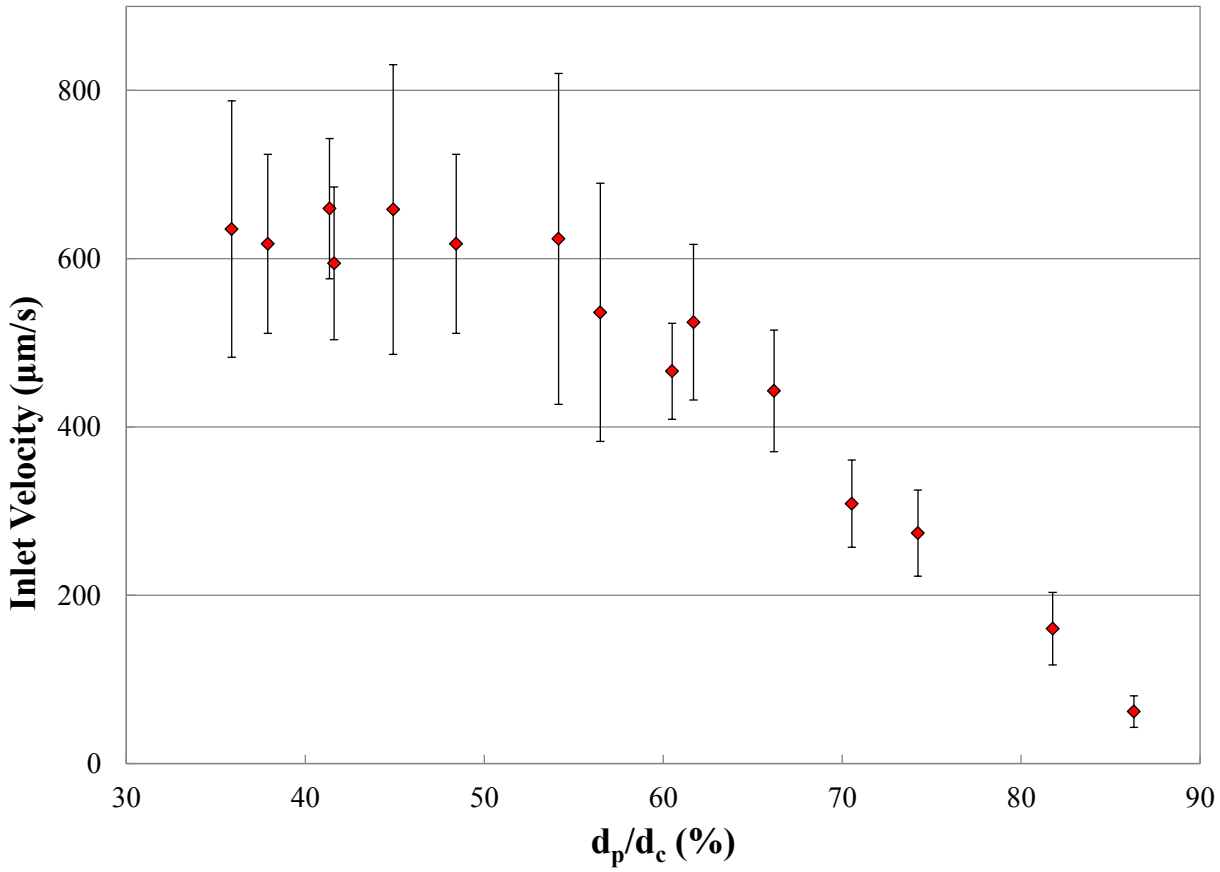

Figure F.1: Full experimental results for the detachment of glass microparticles in a PDMS microchannel, where d_p is the diameter of the glass particle, d_c is the diameter of the PDMS microchannel, and u is the average fluid inlet velocity required for the particle to detach from the bottom of the microchannel. The error on the average value of u is the standard deviation of the data set. For the PDMS microchannel, $d_c = 510\ \mu m$.

Table F.2: Full experimental results for the detachment of glass microparticles in a glass microchannel, where d_p is the diameter of the glass particle, d_c is the diameter of the glass microchannel, and Q is the volumetric flow rate required for the particle to detach from the bottom of the microchannel. The error on the average value of Q is the standard deviation of the data set. For the glass microchannel, $d_c = 500\ \mu m$.

d_p (μm)	d_p/d_c (%)	Detachment Flow Rate, Q (μL/min)							Average Q (μL/min)
183.92	36.78	6.00	7.00	9.50	8.00	7.00	8.50	8.00	7.71 ± 1.15
201.02	40.20	7.00	7.00	8.50	7.50	10.50	11.00	11.00	8.93 ± 1.86
230.12	46.02	8.00	11.00	6.00	10.50	8.50	8.50	6.50	8.43 ± 1.86
263.42	52.68	8.00	10.00	9.00	10.00	7.50	8.50	7.50	8.64 ± 1.07
288.95	57.79	9.00	7.00	9.50	10.00	11.50	8.50	8.50	9.14 ± 1.41
314.64	62.93	7.00	7.50	8.00	5.00	7.00	6.50	8.50	7.07 ± 1.13
329.06	65.81	6.00	5.00	8.50	5.50	5.50	8.00	6.50	6.43 ± 1.34
352.05	70.41	4.00	4.50	6.00	3.50	6.50	5.50	4.00	4.86 ± 1.14
380.21	76.04	7.00	6.00	6.50	6.50	5.00	4.00	4.00	5.57 ± 1.24
408.43	81.69	3.00	6.50	4.00	5.50	3.50	4.00	3.00	4.21 ± 1.32
418.62	83.72	2.00	3.50	2.50	2.50	3.00	3.00	2.50	2.71 ± 0.49

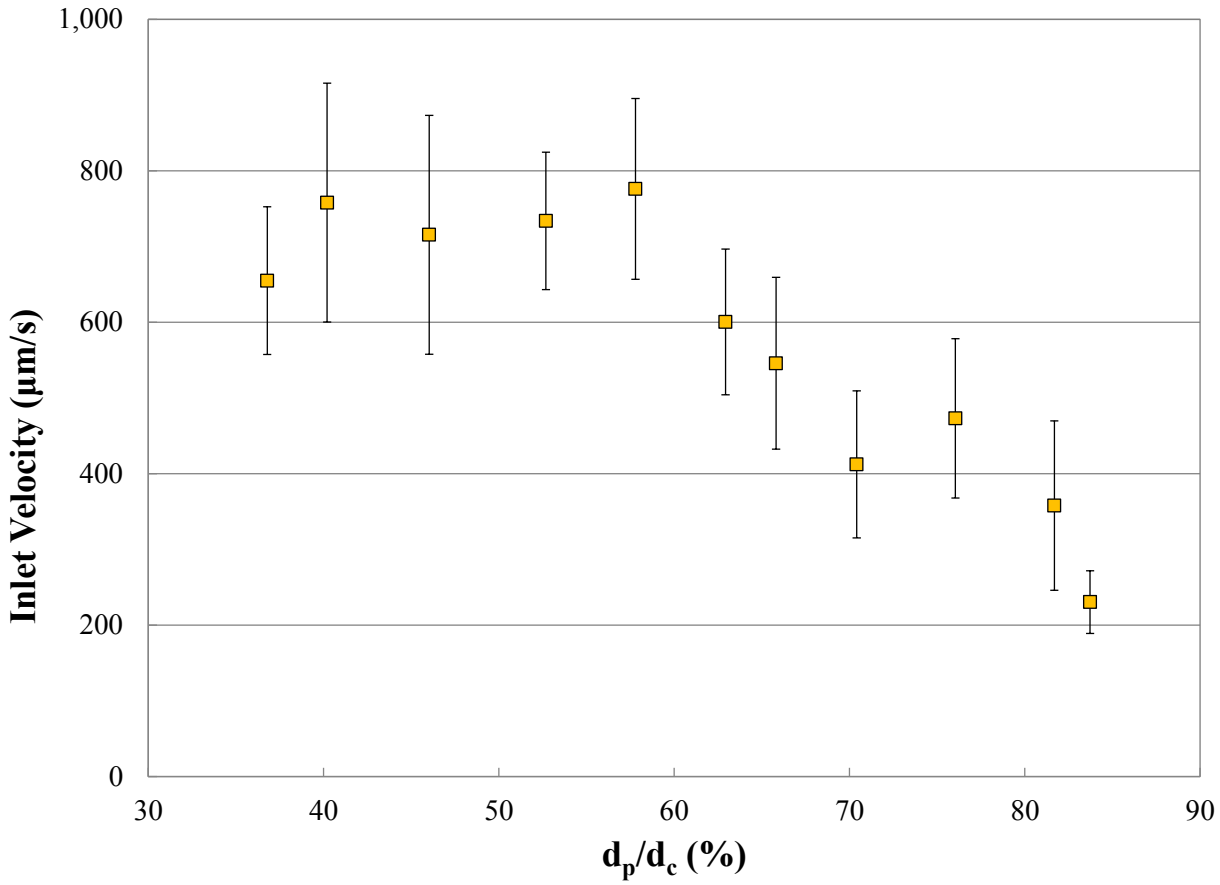

Figure F.2: Full experimental results for the detachment of glass microparticles in a glass microchannel, where d_p is the diameter of the glass particle, d_c is the diameter of the glass microchannel, and u is the average fluid inlet velocity required for the particle to detach from the bottom of the microchannel. The error on the average value of u is the standard deviation of the data set. For the glass microchannel, $d_c = 500\ \mu m$.

Table F.3: Full experimental results for the detachment of PMMA microparticles in a PDMS microchannel, where d_p is the diameter of the PMMA particle, d_c is the diameter of the PDMS microchannel, and Q is the volumetric flow rate required for the particle to detach from the bottom of the microchannel. The error on the average value of Q is the standard deviation of the data set. For the PDMS microchannel, $d_c = 510\ \mu m$.

d_p (μm)	d_p/d_c (%)	Detachment Flow Rate, Q (μL/min)							Average Q (μL/min)
203.54	39.91	0.80	0.50	0.90	0.90	1.00	0.85	1.00	0.85 ± 0.17
226.60	44.43	0.85	0.75	0.80	0.70	0.65	0.60	0.85	0.74 ± 0.10
242.92	47.63	0.70	0.85	0.80	0.95	1.00	0.90	1.15	0.91 ± 0.15
275.28	53.98	1.10	0.80	0.80	0.55	0.80	0.95	0.65	0.81 ± 0.18
294.07	57.66	0.70	0.80	0.50	1.30	0.50	0.85	0.95	0.80 ± 0.28
324.78	63.68	0.60	0.65	0.50	0.50	0.70	0.85	0.65	0.64 ± 0.12
355.54	69.71	0.50	0.35	0.50	0.45	0.60	0.45	0.70	0.51 ± 0.11
376.00	73.73	0.30	0.55	0.40	0.55	0.45	0.60	0.45	0.47 ± 0.10
403.28	79.07	0.40	0.35	0.35	0.45	0.40	0.45	0.35	0.39 ± 0.04
419.62	82.28	0.35	0.35	0.30	0.45	0.30	0.55	0.35	0.38 ± 0.09

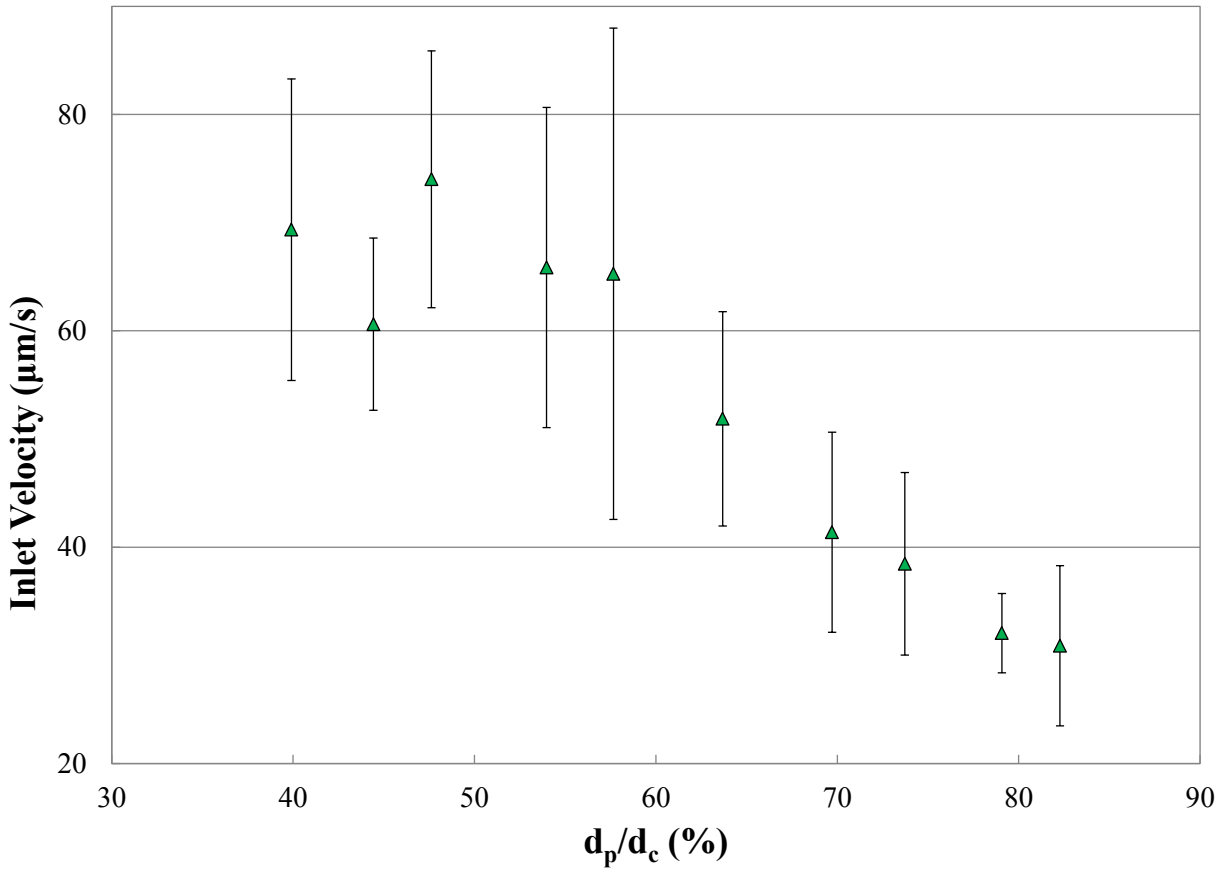

Figure F.3: Full experimental results for the detachment of PMMA microparticles in a PDMS microchannel, where d_p is the diameter of the PMMA particle, d_c is the diameter of the PDMS microchannel, and u is the average fluid inlet velocity required for the particle to detach from the bottom of the microchannel. The error on the average value of u is the standard deviation of the data set. For the PDMS microchannel, $d_c = 510\ \mu m$.

Table F.4: Full experimental results for the detachment of PMMA microparticles in a glass microchannel, where d_p is the diameter of the PMMA particle, d_c is the diameter of the glass microchannel, and Q is the volumetric flow rate required for the particle to detach from the bottom of the microchannel. The error on the average value of Q is the standard deviation of the data set. For the glass microchannel, $d_c = 500\ \mu m$.

d_p (μm)	d_p/d_c (%)	Detachment Flow Rate, Q (μL/min)							Average Q (μL/min)
195.80	39.16	1.10	1.30	1.00	0.60	1.06	0.70	0.75	0.93 ± 0.25
229.05	45.81	0.45	0.90	0.50	0.55	0.35	0.70	0.90	0.62 ± 0.22
252.14	50.43	0.80	0.75	0.75	0.70	0.52	0.72	0.70	0.71 ± 0.09
282.97	56.59	0.42	0.50	1.40	1.10	1.30	0.22	0.34	0.75 ± 0.49
301.75	60.35	0.60	0.56	0.74	1.15	0.52	0.66	0.82	0.72 ± 0.22
324.78	64.96	0.36	1.05	0.65	0.60	1.10	0.70	0.60	0.72 ± 0.26
357.17	71.43	0.50	0.85	0.98	0.28	0.22	0.36	0.60	0.54 ± 0.29
376.00	75.20	0.65	0.75	0.32	0.70	0.80	0.50	0.40	0.59 ± 0.18
398.18	79.64	0.65	0.75	1.00	0.75	0.40	0.85	0.65	0.72 ± 0.19

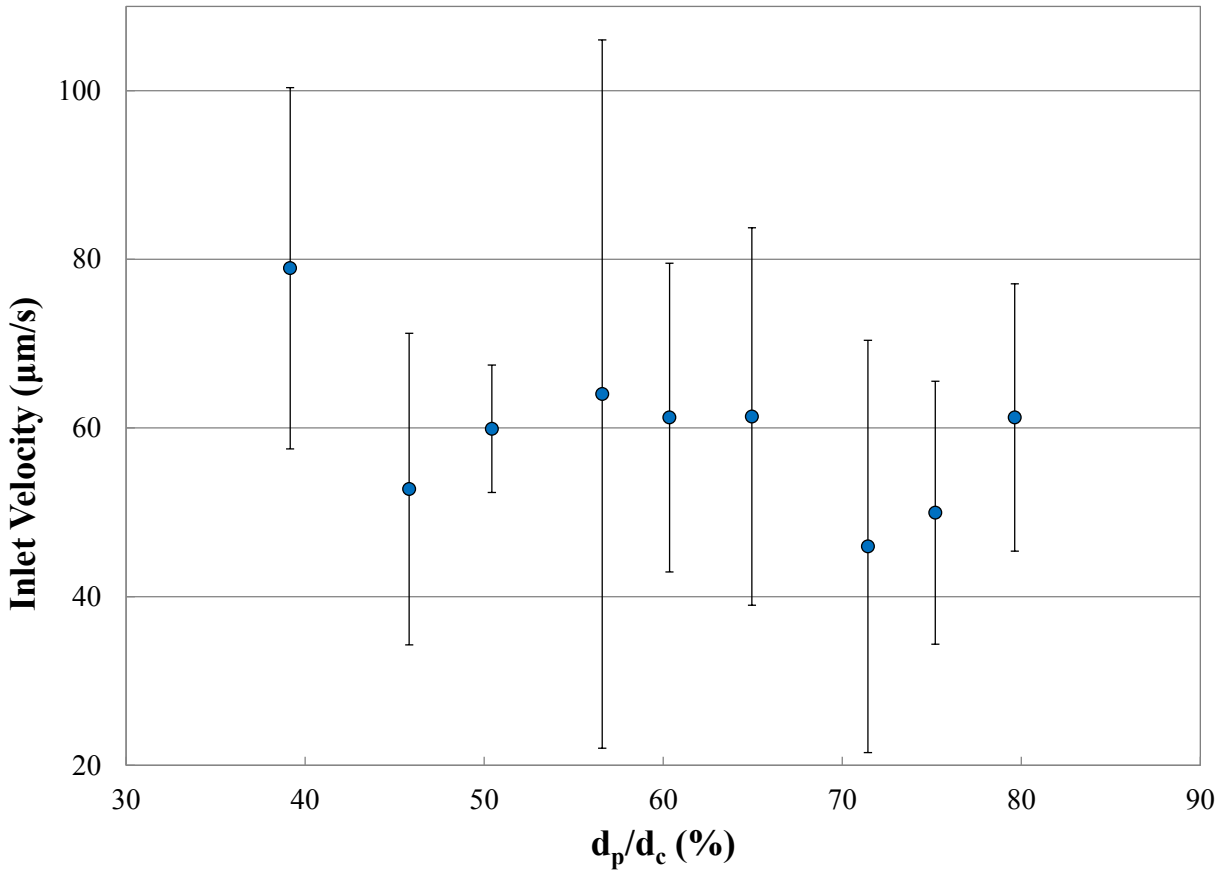

Figure F.4: Full experimental results for the detachment of PMMA microparticles in a glass microchannel, where d_p is the diameter of the PMMA particle, d_c is the diameter of the glass microchannel, and u is the average fluid inlet velocity required for the particle to detach from the bottom of the microchannel. The error on the average value of u is the standard deviation of the data set. For the glass microchannel, $d_c = 500\ \mu m$.

APPENDIX G

Sample Calculations

For the sample calculations, experimental data from the glass particle with a diameter of 308.53 μm in the PDMS channel was used. The values and constants used in the calculations can be found in **Table G.1**, below.

Table G.1: The values and constants used in the sample calculations for a glass particle with a diameter of 308.53 μm in a PDMS channel. All values are given in base SI units.

Symbol	Quantity	Value	Units	Source
d_c	Diameter of the channel	510×10^{-6}	m	Exp.
d_p	Diameter of the particle	308.53×10^{-6}	m	Exp.
E_1	Young's modulus of glass	63×10^{9}	$kg/m \cdot s^2$	COMSOL Mat.
E_2	Young's modulus of PDMS	9.86×10^{5}	$kg/m \cdot s^2$	Exp.
F_D	Drag force	1.30×10^{-8}	$kg \cdot m/s^2$	COMSOL Sim.
F_L	Lift force	4.12×10^{-11}	$kg \cdot m/s^2$	COMSOL Sim.
g	Acceleration due to gravity	9.81	m/s^2	Constant
ν_1	Poisson's ratio of glass	0.2	-	COMSOL Mat.
ν_2	Poisson's ratio of PDMS	0.5	-	COMSOL Mat.
ρ_f	Density of the fluid	998	kg/m^3	Exp.
ρ_p	Density of the particle	2538.6	kg/m^3	Exp.

* COMSOL Sim. indicates that the value was found using the COMSOL simulation detailed in **Appendix A**
* COMSOL Mat. indicates that the value was found in a material library in the COMSOL software, as detailed in **Appendix A**
* Exp. indicates that the value was found experimentally

The goal of these calculations was to find the work of adhesion, W_A, using the moment balance on a rolling particle, shown in Equation 2.18, below.

$$1.74\left(\frac{d_p}{2}\right)F_D = a_{eq}(F_G + F_A - F_L - F_B) \tag{2.18}$$

Both the adhesive forces acting on the particle, F_A, and the particle contact diameter with the channel wall, a_{eq}, are functions of the work of adhesion, as will be shown in the following calculations. But first, the forces acting on the particle must be found.

To calculate the force on the particle due to gravity, **Equation 2.19** was used, as seen below.

$$F_G = \frac{4\pi g \rho_p}{3}\left(\frac{d_p}{2}\right)^3 \tag{2.19}$$

$$F_G = \frac{4\pi\left(9.81\ \frac{m}{s^2}\right)\left(2538.6\ \frac{kg}{m^3}\right)}{3}\left(\frac{308.53\times10^{-6}\ m}{2}\right)^3 = 3.83\times10^{-7}\frac{kg\cdot m}{s^2}$$

To calculate the force on the particle due to buoyancy, **Equation 2.20** was used.

$$F_B = \frac{4\pi g \rho_f}{3}\left(\frac{d_p}{2}\right)^3 \tag{2.20}$$

$$F_B = \frac{4\pi\left(9.81\ \frac{m}{s^2}\right)\left(998\ \frac{kg}{m^3}\right)}{3}\left(\frac{308.53\times10^{-6}\ m}{2}\right)^3 = 1.51\times10^{-7}\frac{kg\cdot m}{s^2}$$

To find the drag and lift forces, the COMSOL model was used, as discussed in **Appendix A**. For this data point, the simulated drag force was $F_D = 1.30\times10^{-8}\ kg\cdot m/s^2$ and the simulated lift force was $F_L = 4.12\times10^{-11}\ kg\cdot m/s^2$. To find the adhesion force as a function of the work of

adhesion, the JKR theory was assumed to be applicable and the equation for the pull-off force was used, as shown in Equation 2.24.

$$F_{A_{JKR}} = 1.5\pi W_A \left(\frac{d_{p,eff}}{2}\right) \tag{2.24}$$

To use this equation, the effective particle diameter must be calculated. To find this quantity, **Equation 2.8**, **Equation 2.9**, and **Equation 2.10** were used.

$$d_{p,eff,sphere} = \left(\frac{1}{d_p} - \frac{1}{d_c}\right)^{-1} \tag{2.9}$$

$$d_{p,eff,sphere} = \left(\frac{1}{308.53 \times 10^{-6}\, m} - \frac{1}{510 \times 10^{-6}\, m}\right)^{-1} = 781.01 \times 10^{-6} m$$

$$d_{p,eff,plane} = d_p \tag{2.10}$$

$$d_{p,eff,plane} = 308.53 \times 10^{-6}\, m$$

$$d_{p,eff} = \frac{\left(d_{p,eff,sphere} - d_{p,eff,plane}\right)}{2} \tag{2.8}$$

$$d_{p,eff} = \frac{(781.01 \times 10^{-6} m - 308.53 \times 10^{-6}\, m)}{2} = 544.77 \times 10^{-6}\, m$$

Once $d_{p,eff}$ was found, the force due to adhesion could be simplified as a function of the work of adhesion, as shown below.

$$F_{A_{JKR}} = 1.5\pi W_A \left(\frac{544.77 \times 10^{-6}\, m}{2}\right) = 1.28 \times 10^{-3} m \cdot W_A$$

To find the contact diameter, a_{eq}, as a function of the work of adhesion, several parameters had to be found first, including the effective particle diameter, which was found above, and the composite Young's modulus. **Equation 2.13** was used to calculate the composite Young's modulus.

$$K = \frac{4}{3(k_1 + k_2)} \tag{2.13}$$

To find k_1 and k_2, the elastic coefficients of the particle and channel materials, respectively, **Equation 2.14** was used.

$$k_i = \frac{1 - \nu_i^2}{E_i} \tag{2.14}$$

$$k_1 = \frac{1 - (0.2)^2}{\left(63 \times 10^9 \ \frac{kg}{m \cdot s^2}\right)} = 1.52 \times 10^{-11} \ \frac{m \cdot s^2}{kg}$$

$$k_2 = \frac{1 - (0.5)^2}{\left(9.86 \times 10^5 \ \frac{kg}{m \cdot s^2}\right)} = 7.61 \times 10^{-7} \ \frac{m \cdot s^2}{kg}$$

Using these values, the composite Young's modulus could be found using **Equation 2.13**, above.

$$K = \frac{4}{3\left(1.52 \times 10^{-11} \ \frac{m \cdot s^2}{kg} + 7.61 \times 10^{-7} \ \frac{m \cdot s^2}{kg}\right)} = 1.75 \times 10^6 \frac{kg}{m \cdot s^2}$$

Once these values were found, the expression for the contact diameter could be simplified, as seen in **Equation 2.12**, below.

$$a_{eq} = \left(\frac{6\pi W_A d_{p,eff}^2}{4K}\right)^{\frac{1}{3}} \tag{2.12}$$

$$a_{eq} = \left(\frac{6\pi W_A (544.77 \times 10^{-6}\, m)^2}{4\left(1.75 \times 10^{6} \frac{kg}{m \cdot s^2}\right)} \right)^{\frac{1}{3}} = 9.28 \times 10^{-5}\ \frac{m \cdot s^{\frac{2}{3}}}{kg^{\frac{1}{3}}} \cdot (W_A)^{\frac{1}{3}}$$

Once the contact diameter and all of the forces were found either as values or as functions of the work of adhesion, the values could be plugged into the moment balance, shown in **Equation 2.18**.

$$1.74 \left(\frac{d_p}{2}\right) F_D = a_{eq}(F_G + F_A - F_L - F_B) \tag{2.18}$$

$$1.74 \left(\frac{308.53 \times 10^{-6}\, m}{2}\right)\left(1.30 \times 10^{-8} \frac{kg \cdot m}{s^2}\right) =$$

$$\left[9.28 \times 10^{-5}\ \frac{m \cdot s^{\frac{2}{3}}}{kg^{\frac{1}{3}}} \cdot (W_A)^{\frac{1}{3}}\right]\left[\left(3.83 \times 10^{-7} \frac{kg \cdot m}{s^2}\right) + (1.28 \times 10^{-3} m \cdot W_A)\right.$$

$$\left. - \left(4.12 \times 10^{-11} \frac{kg \cdot m}{s^2}\right) - \left(1.51 \times 10^{-7} \frac{kg \cdot m}{s^2}\right)\right]$$

Simplified, this expression becomes

$$3.48 \times 10^{-12}\ \frac{kg \cdot m^2}{s^2} =$$

$$\left[9.28 \times 10^{-5}\ \frac{m \cdot s^{\frac{2}{3}}}{kg^{\frac{1}{3}}} \cdot (W_A)^{\frac{1}{3}}\right]\left[\left(2.32 \times 10^{-7} \frac{kg \cdot m}{s^2}\right) + (1.28 \times 10^{-3} m \cdot W_A)\right]$$

In order to find the work of adhesion, the difference between the left and right sides of the moment balance was calculated and squared for all of the particle diameters of a given material pairing. These squared differences were then summed and Excel's solver function was

used to minimize the sum. Because these numbers are within the range of Excel's tolerance levels, each squared difference was multiplied by a factor of 10^{25} so that a solution could be found. For the material pairing of glass particles in PDMS channels, the work of adhesion was found to be $W_A = 0.177 \times 10^{-4}\, kg/s^2$, or $177\, \mu N/m$. As a visual representation of this process, the left and right hand sides of the moment balance, representing the effective drag moment and the moment due to friction, respectively, were plotted against each other for each material pairing. In this visualization, the work of adhesion can be thought of as a fitting parameter, causing the friction moment to equal the drag moment, forcing the moment balance to be true. These plots can be found in **Appendix H** for each material pairing.

Once the work of adhesion was found, the rolling moment was calculated to determine if the moment balance approach was correct. The expression for the rolling moment is shown in **Equation 2.6**, below.

$$RM = \frac{F_D\left(1.399\ \frac{d_p}{2} - \alpha\right)}{(F_A + F_G - F_B - F_L)\frac{a_{eq}}{2}} \tag{2.6}$$

All of the variables in this equation were calculated previously with the exception of the deformation of the particle, α, which was calculated using **Equation 2.7**.

$$\alpha = \frac{d_{p,eff}}{2} - \left[\left(\frac{d_{p,eff}}{2}\right)^2 - \left(\frac{a_{eq}}{2}\right)^2\right]^{\frac{1}{2}} \tag{2.7}$$

$$\alpha = \frac{544.77 \times 10^{-6}\, m}{2} - \left[\left(\frac{544.77 \times 10^{-6}\, m}{2}\right)^2 - \left(\frac{9.28 \times 10^{-5}\ \frac{m \cdot s^{\frac{2}{3}}}{kg^{\frac{1}{3}}} \cdot \left(0.177 \times 10^{-4}\, \frac{kg}{s^2}\right)^{\frac{1}{3}}}{2}\right)^2\right]^{\frac{1}{2}}$$

$$= 1.25 \times 10^{-6} m$$

Using this value, the rolling moment was calculated.

$$RM = \left[1.30 \times 10^{-8}\, \frac{kg \cdot m}{s^2}\left(1.399\ \frac{308.53 \times 10^{-6}\, m}{2} - 1.25 \times 10^{-6} m\right)\right] \cdot \left\{\left[\left(1.28 \times 10^{-3} m \cdot 0.177 \times 10^{-4}\, \frac{kg}{s^2}\right) + \left(3.83 \times 10^{-7}\, \frac{kg \cdot m}{s^2}\right) - \left(1.51 \times 10^{-7}\, \frac{kg \cdot m}{s^2}\right) - \left(4.12 \times 10^{-11}\, \frac{kg \cdot m}{s^2}\right)\right]\left[\frac{9.28 \times 10^{-5}\ \frac{m \cdot s^{\frac{2}{3}}}{kg^{\frac{1}{3}}} \cdot \left(0.177 \times 10^{-4}\, \frac{kg}{s^2}\right)^{\frac{1}{3}}}{2}\right]\right\}^{-1}$$

$$RM = 2.33$$

As mentioned previously, if the rolling moment was greater than one, which it was, the particle will detach from the bottom of the channel through a rolling motion, making the moment balance applicable for this system.

APPENDIX H

Results of Calculations

Table H.1: The material properties and dimensions used in the calculations. All values are given in base SI units. All quantities that originated from the COMSOL Multiphysics 5.1 software are detailed in **Appendix A**.

Symbol	Material	Quantity	Value	Units	Source
d_c	PDMS	Diameter of the channel	510×10^{-6}	m	Exp.
d_c	Glass	Diameter of the channel	500×10^{-6}	m	Spec.
E_i	PDMS	Young's modulus	9.86×10^5	$kg/m \cdot s^2$	Exp.
E_i	Glass	Young's modulus	63×10^9	$kg/m \cdot s^2$	COMSOL
E_i	PMMA	Young's modulus	3.0×10^9	$kg/m \cdot s^2$	COMSOL
ν_i	PDMS	Poisson's ratio	0.5	-	COMSOL
ν_i	PDMS	Poisson's ratio	0.2	-	COMSOL
ν_i	PMMA	Poisson's ratio	0.4	-	COMSOL
ρ_p	Glass	Density of the particle	2538.6	kg/m^3	Exp.
ρ_p	PMMA	Density of the particle	1184.4	kg/m^3	Exp.
ρ_f	Water	Density of the fluid	998	kg/m^3	Exp.

* COMSOL indicates that the value was found in a material library in the COMSOL software
* Exp. indicates that the value was found experimentally
* Spec. indicates that the value was taken as a product specification from the manufacturer

Table H.2: The intermediate values calculated for each material or material pairing. For the material pairings, the particle material is listed first and the channel material is listed second. The details of these calculations can be found in **Appendix G**.

Symbol	Material	Quantity	Value	Units
k_i	PDMS	Elastic coefficient	7.61×10^{-7}	$m \cdot s^2/kg$
k_i	Glass	Elastic coefficient	1.52×10^{-11}	$m \cdot s^2/kg$
k_i	PMMA	Elastic coefficient	2.80×10^{-10}	$m \cdot s^2/kg$
K	Glass/PDMS	Composite Young's modulus	1.75×10^{6}	$kg/m \cdot s^2$
K	Glass/Glass	Composite Young's modulus	4.38×10^{10}	$kg/m \cdot s^2$
K	PMMA/PDMS	Composite Young's modulus	1.75×10^{6}	$kg/m \cdot s^2$
K	PMMA/Glass	Composite Young's modulus	4.52×10^{9}	$kg/m \cdot s^2$

Table H.3: The forces acting on glass microparticles in a PDMS channel at the point of particle detachment. For the PDMS microchannel, $d_c = 510\ \mu m$.

d_p (μm)	d_p/d_c (%)	F_G (μN)	F_B (μN)	F_D (μN)	F_L (μN)	F_A (μN)
183.03	35.89	0.080	0.031	0.0030	1.87E-05	0.098
193.32	37.91	0.094	0.037	0.0034	2.04E-05	0.105
210.91	41.35	0.122	0.048	0.0046	2.40E-05	0.119
212.21	41.61	0.125	0.049	0.0042	2.53E-05	0.120
229.05	44.91	0.157	0.062	0.0059	2.83E-05	0.135
247.00	48.43	0.196	0.077	0.0071	3.89E-05	0.152
276.18	54.15	0.275	0.108	0.0108	6.05E-05	0.183
288.08	56.49	0.312	0.123	0.0110	6.28E-05	0.198
308.53	60.50	0.383	0.151	0.0130	4.12E-05	0.227
314.64	61.69	0.406	0.160	0.0164	1.46E-05	0.237
337.58	66.19	0.502	0.197	0.0198	3.84E-05	0.279
359.75	70.54	0.607	0.239	0.0206	3.68E-05	0.330
378.58	74.23	0.708	0.278	0.0269	-1.82E-05	0.386
416.99	81.76	0.945	0.372	0.0392	-2.96E-07	0.564
440.15	86.30	1.112	0.437	0.0317	-4.64E-05	0.763

Table H.4: The contact diameter (a_{eq}), particle deformation (α), and rolling moment (RM) calculated for glass microparticles in a PDMS channel at the point of particle detachment.

d_p (μm)	d_p/d_c (%)	a_{eq} (m)	α (m)	RM
183.03	35.89	2.97E-06	9.40E-09	1.759
193.32	37.91	3.12E-06	9.64E-09	1.806
210.91	41.35	3.39E-06	1.00E-08	2.067
212.21	41.61	3.41E-06	1.01E-08	1.880
229.05	44.91	3.67E-06	1.05E-08	2.251
247.00	48.43	3.97E-06	1.09E-08	2.276
276.18	54.15	4.51E-06	1.16E-08	2.638
288.08	56.49	4.76E-06	1.19E-08	2.412
308.53	60.50	5.21E-06	1.25E-08	2.335
314.64	61.69	5.36E-06	1.26E-08	2.790
337.58	66.19	5.97E-06	1.33E-08	2.680
359.75	70.54	6.68E-06	1.41E-08	2.226
378.58	74.23	7.41E-06	1.49E-08	2.357
416.99	81.76	9.55E-06	1.69E-08	2.106
440.15	86.30	1.17E-05	1.86E-08	1.163

Table H.5: The forces acting on glass microparticles in a glass channel at the point of particle detachment. For the glass microchannel, $d_c = 500\ \mu m$.

d_p (μm)	d_p/d_c (%)	F_G (μN)	F_B (μN)	F_D (μN)	F_L (μN)	F_A (μN)
183.92	36.78	0.081	0.032	0.0032	2.32E-05	4.004
201.02	40.20	0.106	0.042	0.0048	2.30E-05	4.529
230.12	46.02	0.159	0.062	0.0109	6.82E-05	5.535
263.42	52.68	0.238	0.094	0.0112	7.13E-05	6.915
288.95	57.79	0.315	0.124	0.0173	8.25E-05	8.208
314.64	62.93	0.406	0.160	0.0201	5.01E-05	9.809
329.06	65.81	0.465	0.183	0.0235	7.83E-05	10.890
352.05	70.41	0.569	0.224	0.0269	2.46E-05	13.000
380.21	76.04	0.717	0.282	0.0549	1.26E-04	16.586
408.43	81.69	0.888	0.349	0.0847	5.18E-05	22.247
418.62	83.72	0.957	0.376	0.0739	9.27E-05	25.215

Table H.6: The contact diameter (a_{eq}), particle deformation (α), and rolling moment (RM) calculated for glass microparticles in a glass channel at the point of particle detachment.

d_p (μm)	d_p/d_c (%)	a_{eq} (m)	α (m)	RM
183.92	36.78	3.52E-07	1.30E-10	0.583
201.02	40.20	3.82E-07	1.36E-10	0.766
230.12	46.02	4.36E-07	1.45E-10	1.430
263.42	52.68	5.06E-07	1.56E-10	1.154
288.95	57.79	5.67E-07	1.65E-10	1.465
314.64	62.93	6.39E-07	1.75E-10	1.380
329.06	65.81	6.85E-07	1.82E-10	1.412
352.05	70.41	7.71E-07	1.93E-10	1.290
380.21	76.04	9.07E-07	2.09E-10	1.893
408.43	81.69	1.10E-06	2.31E-10	1.926
418.62	83.72	1.20E-06	2.40E-10	1.400

Table H.7: The forces acting on PMMA microparticles in a PDMS channel at the point of particle detachment. For the PDMS microchannel, $d_c = 510\ \mu m$.

d_p (μm)	d_p/d_c (%)	F_G (μN)	F_B (μN)	F_D (μN)	F_L (μN)	F_A (μN)
203.54	39.91	0.051	0.043	0.0004	-2.83E-07	0.054
226.60	44.43	0.071	0.060	0.0005	1.23E-07	0.063
242.92	47.63	0.087	0.073	0.0008	-7.30E-07	0.070
275.28	53.98	0.127	0.107	0.0011	3.10E-07	0.087
294.07	57.66	0.155	0.130	0.0015	-7.47E-08	0.099
324.78	63.68	0.208	0.176	0.0019	-4.69E-06	0.122
355.54	69.71	0.273	0.230	0.0026	-2.12E-06	0.153
376.00	73.73	0.323	0.272	0.0036	9.86E-07	0.180
403.28	79.07	0.399	0.336	0.0054	-6.83E-06	0.232
419.62	82.28	0.450	0.379	0.0081	-5.86E-07	0.278

Table H.8: The contact diameter (a_{eq}), particle deformation (α), and rolling moment (RM) calculated for PMMA microparticles in a PDMA channel at the point of particle detachment.

d_p (μm)	d_p/d_c (%)	a_{eq} (m)	α (m)	RM
203.54	39.91	2.56E-06	6.03E-09	0.779
226.60	44.43	2.84E-06	6.36E-09	0.782
242.92	47.63	3.05E-06	6.59E-09	1.061
275.28	53.98	3.52E-06	7.07E-09	1.160
294.07	57.66	3.82E-06	7.37E-09	1.277
324.78	63.68	4.39E-06	7.90E-09	1.285
355.54	69.71	5.11E-06	8.53E-09	1.289
376.00	73.73	5.71E-06	9.01E-09	1.424
403.28	79.07	6.76E-06	9.81E-09	1.522
419.62	82.28	7.62E-06	1.04E-08	1.799

Table H.9: The forces acting on PMMA microparticles in a glass channel at the point of particle detachment. For the glass microchannel, $d_c = 500\ \mu m$.

d_p (μm)	d_p/d_c (%)	F_G (μN)	F_B (μN)	F_D (μN)	F_L (μN)	F_A (μN)
252.14	50.43	0.098	0.082	0.0008	-3.90E-08	0.839
357.17	71.43	0.277	0.234	0.0033	-6.49E-06	1.773
195.80	39.16	0.046	0.038	0.0005	1.19E-06	0.571
301.75	60.35	0.167	0.141	0.0016	-1.44E-06	1.172
398.18	79.64	0.384	0.324	0.0110	-6.43E-06	2.595
229.05	45.81	0.073	0.062	0.0005	-4.46E-08	0.719
376.00	75.20	0.323	0.272	0.0053	-2.80E-06	2.086
324.78	64.96	0.208	0.176	0.0024	-1.96E-07	1.380
282.97	56.59	0.138	0.116	0.0013	6.32E-07	1.031

Table H.10: The contact diameter (a_{eq}), particle deformation (α), and rolling moment (RM) calculated for PMMA microparticles in a glass channel at the point of particle detachment.

d_p (μm)	d_p/d_c (%)	a_{eq} (m)	α (m)	RM
252.14	50.43	5.21E-07	1.78E-10	0.614
357.17	71.43	8.58E-07	2.29E-10	1.050
195.80	39.16	4.03E-07	1.57E-10	0.544
301.75	60.35	6.51E-07	1.99E-10	0.892
398.18	79.64	1.11E-06	2.60E-10	2.078
229.05	45.81	4.70E-07	1.69E-10	0.458
376.00	75.20	9.56E-07	2.42E-10	1.368
324.78	64.96	7.26E-07	2.10E-10	1.078
282.97	56.59	5.98E-07	1.91E-10	0.818

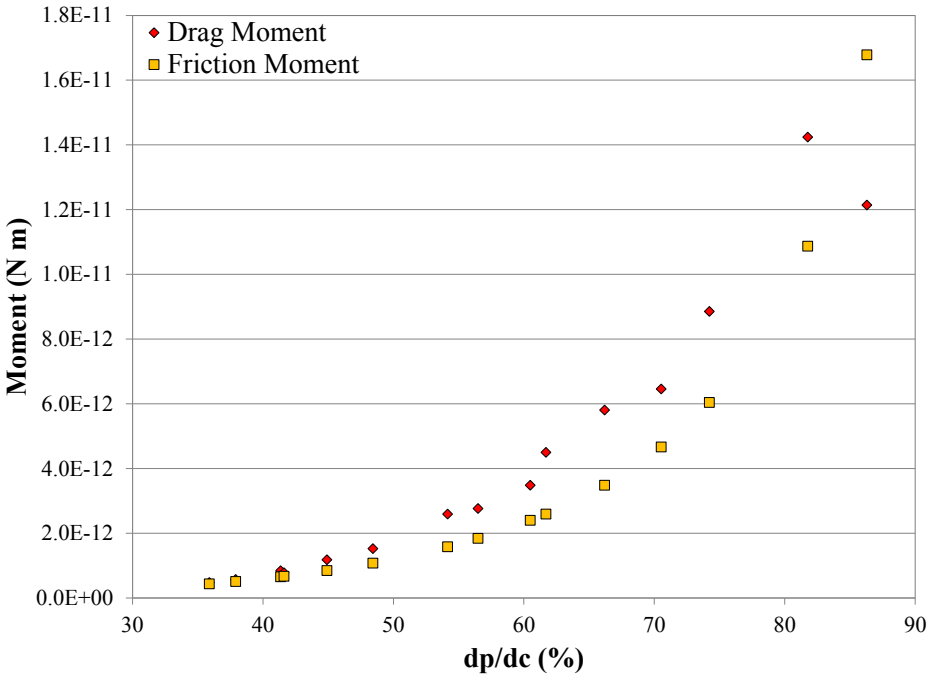

Figure H.1: The drag and friction moments acting on glass microparticles in a PDMS channel at the point of particle detachment. The work of adhesion acts as a fitting parameter to match the friction moment to the drag moment. In this case, the work of adhesion is $W_A = 177\ \mu N/m$.

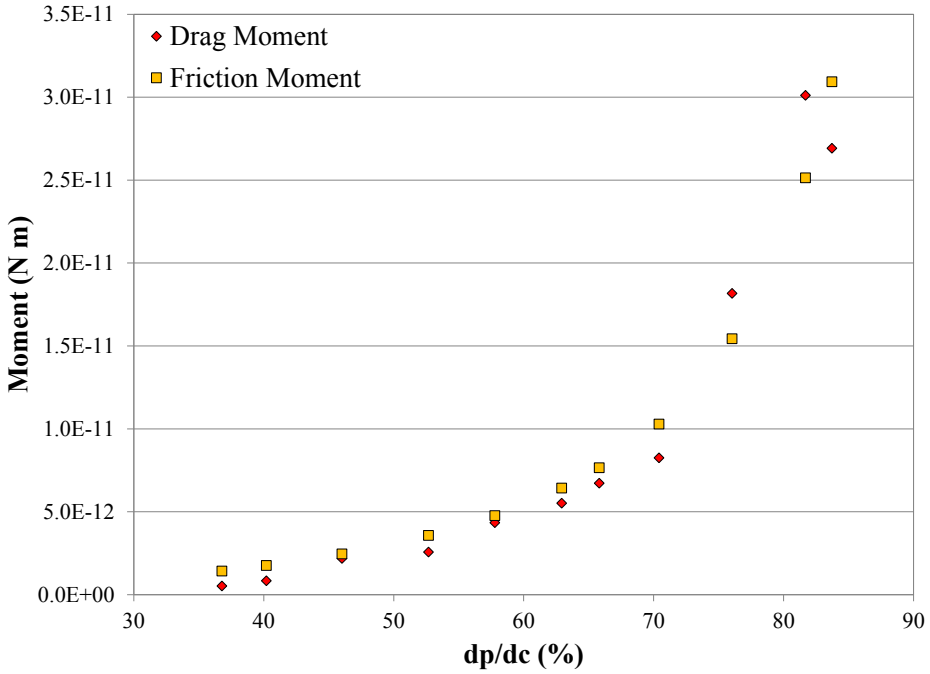

Figure H.2: The drag and friction moments acting on glass microparticles in a glass channel at the point of particle detachment. The work of adhesion acts as a fitting parameter to match the friction moment to the drag moment. In this case, the work of adhesion is $W_A = 7{,}157\ \mu N/m$.

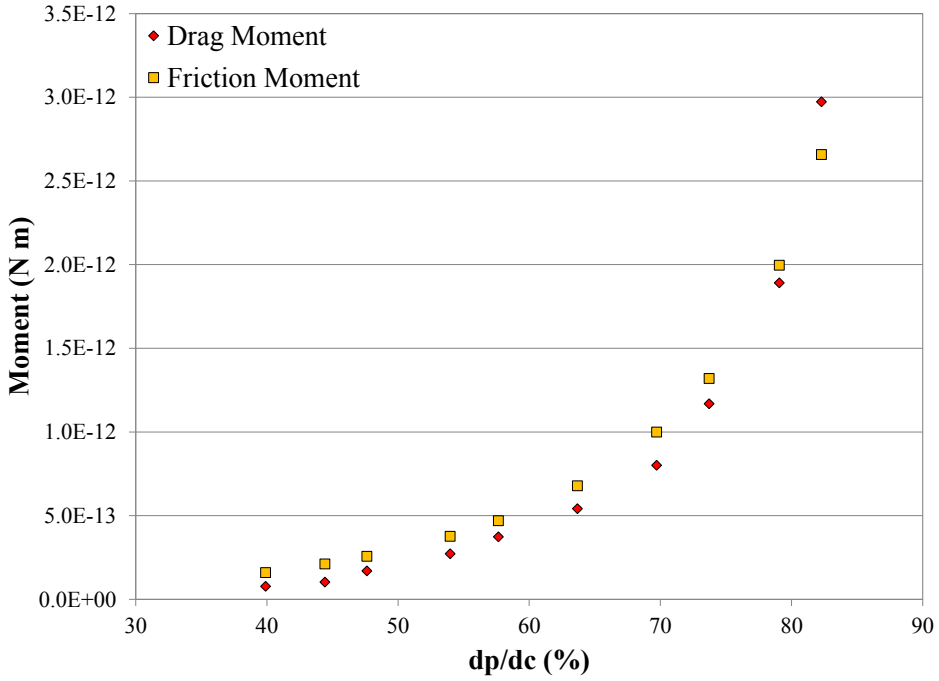

Figure H.3: The drag and friction moments acting on PMMA microparticles in a PDMS channel at the point of particle detachment. The work of adhesion acts as a fitting parameter to match the friction moment to the drag moment. In this case, the work of adhesion is $W_A = 85\ \mu N/m$.

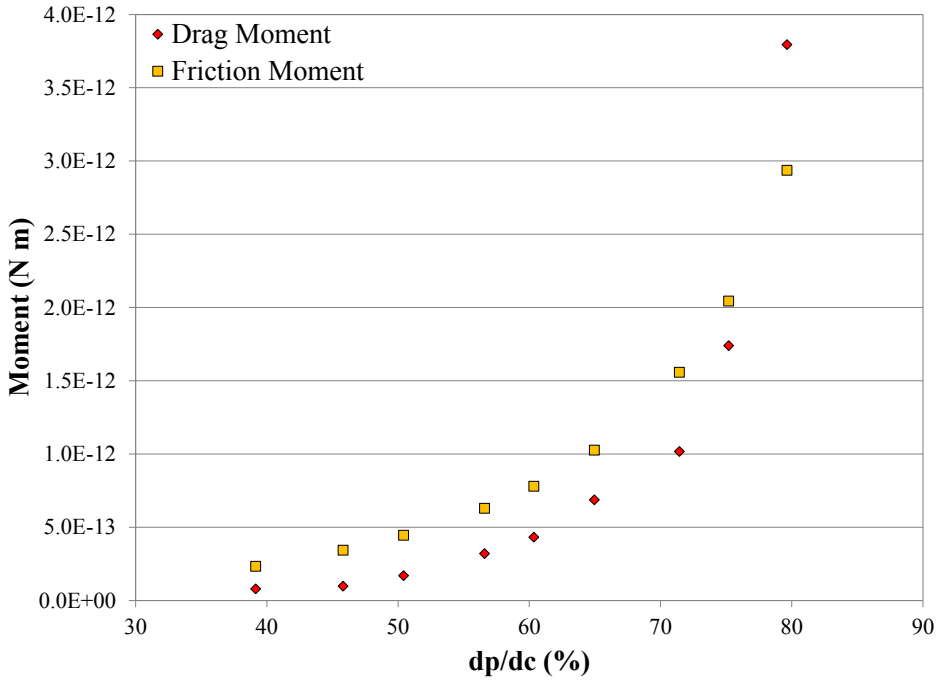

Figure H.4: The drag and friction moments acting on PMMA microparticles in a glass channel at the point of particle detachment. The work of adhesion acts as a fitting parameter to match the friction moment to the drag moment. In this case, the work of adhesion is $W_A = 936\ \mu N/m$.